

Optimization of build parameters of FDM 3D printing to reduce
build time and increase its mechanical Strength



Author

ABDUL SAMAD RAFIQUE

Reg. Number

328390

Supervisor

DR. ADNAN MUNIR

DEPARTMENT OF MECHANICAL ENGINEERING
SCHOOL OF MECHANICAL & MANUFACTURING ENGINEERING
NATIONAL UNIVERSITY OF SCIENCES AND TECHNOLOGY
ISLAMABAD
SEPTEMBER, 2023

Optimization of build parameters of FDM 3D printing to reduce build
time and increase its mechanical Strength

Author

ABDUL SAMAD RAFIQUE

Regn. Number

328390

A thesis submitted in partial fulfillment of the requirements for the degree of
MS Mechanical Engineering

Thesis Supervisor:

DR. ADNAN MUNIR

Thesis Supervisor's Signature: _____



DEPARTMENT OF MECHANICAL ENGINEERING
SCHOOL OF MECHANICAL & MANUFACTURING ENGINEERING
NATIONAL UNIVERSITY OF SCIENCES AND TECHNOLOGY,
ISLAMABAD
SEPTEMBER, 2023



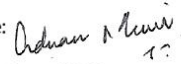
National University of Sciences & Technology (NUST)
MASTER'S THESIS WORK

We hereby recommend that the dissertation prepared under our supervision by: Abdul samad Rafique (00000328390)
Titled: Optimization Of Build Parameters of FDM 3D Printing to reduce Build Time & increase Part Quality, be accepted in
partial fulfillment of the requirements for the award of MS in Mechanical Engineering degree.

Examination Committee Members

- | | | |
|----|----------------------------|--|
| 1. | Name: Emad Ud Din | Signature:  |
| 2. | Name: Muhammad Safdar | Signature:  |
| 3. | Name: Muhammad Salman Khan | Signature:  |

Supervisor: Adnan Munir

Signature: 
Date: 05 - Sep - 2023



Head of Department

05 - Sep - 2023

Date

COUNTERSIGNED

05 - Sep - 2023

Date



Dean/Principal

Thesis Acceptance Certificate

Certified that final copy of MS thesis written by Abdul Samad Rafique Registration No. 322390, of SMME has been vetted by undersigned, found complete in all respects as per NUST Statutes / Regulations, is free of plagiarism, errors, and mistakes and is accepted as partial fulfillment for award of MS degree. It is further certified that necessary amendments as pointed out by GEC members of the scholar have also been incorporated in the said thesis.

Signature: Adnan Munir
Name of Supervisor: Dr Adnan Munir
Date: 13-9-23

Signature (HOD): Emad
Date: 13-9-23

Signature (Principal): [Signature]
Date: 13-9-23

Certificate for Plagiarism

It is certified that MS Thesis Titled: Optimization of Build Parameters of FDM 3D printing by to reduce Build time and increase Part Strength
Abdul Samad Rafique has been examined by me. I undertake the follows:

- a. Thesis has significant new work/knowledge as compared already published or are under consideration to be published elsewhere. No sentence, equation, diagram, table, paragraph, or section has been copied verbatim from previous work unless it is placed under quotation marks and duly referenced.
- b. The work presented is original and own work of the author (i.e., there is no plagiarism). No ideas, processes, results, or words of others have been presented as Author own work.
- c. There is no fabrication of data or results which have been compiled/analyzed.
- d. There is no falsification by manipulating research materials, equipment, or processes, or changing or omitting data or results such that the research is not accurately represented in the research record.
- e. The thesis has been checked using TURNITIN (copy of originality report attached) and found within limits as per HEC plagiarism Policy and instructions issued from time to time.

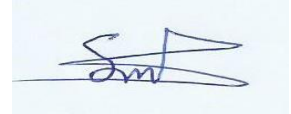
Name & Signature of Supervisor

Signature: Dr Adnan Munir

Dr. Adnan Munir
Assistant Professor
NUST School of Mechanical &
Manufacturing Engineering,
Islamabad, Pakistan

Declaration

I certify that this research work titled “*Optimization of build parameters of FDM 3D printing to reduce build time and increase its mechanical Strength*” is my own work. The work has not been presented elsewhere for assessment. The material that has been used from other sources it has been properly acknowledged / referred.

A handwritten signature in blue ink, appearing to read 'S. Rafique', is placed on a light blue rectangular background.

Signature of Student

ABDUL SAMAD RAFIQUE

2020-NUST-MS-Mech-328390

Copyright Statement

- Copyright in text of this thesis rests with the student author. Copies (by any process) either in full, or of extracts, may be made only in accordance with instructions given by the author and lodged in the Library of NUST School of Mechanical & Manufacturing Engineering (SMME). Details may be obtained by the Librarian. This page must form part of any such copies made. Further copies (by any process) may not be made without the permission (in writing) of the author.
- The ownership of any intellectual property rights which may be described in this thesis is vested in NUST School of Mechanical & Manufacturing Engineering, subject to any prior agreement to the contrary, and may not be made available for use by third parties without the written permission of the SMME, which will prescribe the terms and conditions of any such agreement.
- Further information on the conditions under which disclosures and exploitation may take place is available from the Library of NUST School of Mechanical & Manufacturing Engineering, Islamabad.

Acknowledgements

I am thankful to my Creator Allah Subhana-Watala to have guided me throughout this work at every step and for every new thought which You setup in my mind to improve it. Indeed I could have done nothing without Your priceless help and guidance. Whosoever helped me throughout the course of my thesis, whether my parents or any other individual was Your will, so indeed none be worthy of praise but You.

I am profusely thankful to my beloved parents who raised me when I was not capable of walking and continued to support me throughout in every department of my life.

I would also like to express special thanks to my supervisor Dr. Adnan Munir & external supervisor Dr A. A. Khurram for his help throughout my thesis. I would also like to pay special thanks to Dr M. Salman Khan for his tremendous support and cooperation. Their invaluable assistance played a pivotal role in the successful completion of my thesis in DME labs. I appreciate his patience and guidance throughout the whole thesis.

I would also like to thank Dr. Emad and Dr. M. Safdar for being on my thesis guidance and evaluation committee.

Finally, I would like to express my gratitude to all the individuals who have rendered valuable assistance to my study.

*Dedicated to my exceptional parents and adored siblings whose
tremendous support and cooperation led me to this wonderful
accomplishment.*

Abstract

During 3D printing part, many process parameters of the printer are required to be considered that affect the mechanical properties such as part strength. This research investigates the influence of layer height and print speed variations on the strength and quality of Fused Deposition Modelling (FDM) parts. The article shows the realized results of experiments and measurements of mechanical strengths, artifact dimensional accuracy, surface roughness and hatch distances. Proper selection of printing parameters is essential for achieving desired mechanical properties in 3D printed parts. The study employs Design of Experiments (DOEs) on different shaped geometries by using full factorial methodology to select the significant parameters for further research. A comprehensive test artifact is used to assess printer performance and dimensional limits. The test artifact, designed with various combinations of print speed and layer height, is subjected to 3D scanning to create 3D deviation maps, perform 3D comparisons, and calculate percentage error. Tensile tests and 3-point bend tests were conducted on test specimens, employing combinations of three distinct layer heights and print speeds. These tests were carried out following ASTM standards D 638 and D 790 to evaluate the tensile and flexure strengths, respectively. The outcomes indicate that extra fine layer heights and the lower print speeds yield higher strength and dimensional accuracy. Surface roughness and hatch distance analyses exhibit consistent patterns across both the tensile and 3-point bend tests. The results contribute to the exploration of FDM parameters for specific applications and the progress of additive manufacturing methodologies.

Key Words: *Additive Manufacturing (AM), Fused Deposition Modelling (FDM), Design of Experiments (DOEs), Dimensional accuracy, Tensile testing, 3 point bending test, Surface roughness*

Table of Contents

Declaration	iv
Copyright Statement	v
Acknowledgements	vi
Abstract	viii
Table of Contents.....	ix
List of Figures	x
List of Tables.....	xi
CHAPTER 1: INTRODUCTION.....	1
1.1 Fused Deposition Modelling	2
1.2 Critical 3D printing parameters in FDM	3
1.3 Effects of FDM Parameters on Part Quality:	4
CHAPTER 2: Material & Methodology	6
2.1 Tensile Test.....	7
2.2 3-Point bending test.....	8
2.3 Artifacts 3D Scanning	9
2.4 Surface Roughness & Hatch Distance.....	11
CHAPTER 3: RESULTS & DISCUSSIONS	12
3.1 Design of Experiments (DoE)	12
3.1.1 Parameters Selection.....	12
3.1.2 Models	13
3.1.3 Responses Measurements	14
3.1.4 Analysis of Variance (ANOVA) Results	15
3.1.5 Significant parameters	17
3.2 Test Artifact Results.....	18
3.2.1 Measured Values	18
3.2.2 3D Compare.....	20
3.2.3 Percentage Error	23
3.3 Tensile Test ASTM D-638.....	30
3.4 3-Point Bend Test ASTM D-790	34
3.5 Surface Roughness	37
3.5.1 Tensile Testing Specimen	37
3.5.2 3-Point Bending Specimen	44
CHAPTER 4: CONCLUSION	49
REFERENCES	50

List of Figures

Figure 2.1: ASTM D-638 TYPE IV specimen drawing	7
Figure 2.2: ASTM D790-10 specimen drawing	8
Figure 2.3: Test Artifacts Dimensions	9
Figure 2.4: Test Artifact Geometries	10
Figure 2.5: Olympus DSX 1000 Digital microscope	11
Figure 3.1: DOE Models	14
Figure 3.2: Boundary Dimensions Error % Deviation.....	23
Figure 3.3: Centre hole Dimensions Error % Deviation	24
Figure 3.4: Ramp Dimensions Error % Deviation.....	24
Figure 3.5: Circular Hole Error % Deviation.....	25
Figure 3.6: Diagonal Pins Dimensions Error % Deviation	25
Figure 3.7: Rectangular Pins Dimensions Error % Deviation	26
Figure 3.8: Rectangular Pins Slot Dimensions Error % Deviation	27
Figure 3.9: Circular Pins Dimensions Error % Deviation	27
Figure 3.10: Circular Pins Slot Dimensions Error % Deviation	28
Figure 3.11: Rectangular plate Dimensions Error % Deviation	28
Figure 3.12: Rectangular plate Angle (degrees) Error % Deviation	29
Figure 3.13: Book Shaped Dimension & Angle Error % Deviation.....	29
Figure 3.14: Round Ball Diameter Error % Deviation	30
Figure 3.15: Ultimate Tensile Strength D 638 Graph.....	33
Figure 3.16: Tensile Testing Elongation (%) Graph.....	33
Figure 3.17: 3-Point Bending Flexure Strength Graph	36
Figure 3.18: 3-Point Bending Elongation (%) Graph	37
Figure 3.19: Tensile Testing Specimen Top Surface Roughness	38
Figure 3.20: Tensile Testing Specimen Side Surface Roughness	39
Figure 3.21: Tensile Testing Specimen Top Surface Hatch Distances	40
Figure 3.22: Tensile Testing Specimen Side Surface Hatch Distances	40
Figure 3.23: 3-Point Bending Specimen Top Surface Roughness	45
Figure 3.24: 3-Point Bending Specimen Side Surface Roughness	45
Figure 3.25: 3-Point Bending Specimen Top Surface Hatch Distances	46
Figure 3.26: 3-Point Bending Specimen Side Surface Hatch Distances.....	46

List of Tables

Table 2.1: ABS Material data	6
Table 2.2: 3D Printer Specification & Fixed Parameters for Tensile & 3-Point bend test specimens.....	6
Table 2.3: Parameters of samples for Tensile & 3-Point bend test specimens	8
Table 3.1: Responses	12
Table 3.2: Selected Parameters.....	12
Table 3.3: Full Factorial 2 ⁵ DOE Experiments.....	14
Table 3.4: ANOVA table for Build time	16
Table 3.5: Build Time Response Model & its Contributions	17
Table 3.6: Artifacts Measured Values	18
Table 3.7: 3D Deviation Map	21
Table 3.8: 3D Compare Peak Tolerances	22
Table 3.9: 3D Compare Tolerances Values	22
Table 3.7: Tensile Testing Experimental Data	31
Table 3.8: Tensile Testing Stress Strain Graph	32
Table 3.9: 3-Point Bending D-790 Experimental Data.....	34
Table 3.10: 3-Point Bending Stress Strain Graph.....	35
Table 3.11: Tensile Testing Specimen Surface Roughness & Hatch Distance.....	38
Table 3.12: Tensile Testing Specimen Top Surface Hatch Distances	42
Table 3.13: Tensile Testing Specimen Side Surface Hatch Distances.....	43
Table 3.14: 3-Point Bending Specimen Surface Roughness & Hatch Distance	44
Table 3.15: 3-Point Bending Specimen Top Surface Hatch Distances.....	47
Table 3.16: 3-Point Bending Specimen Side Surface Hatch Distances	48

CHAPTER 1: INTRODUCTION

Additive Manufacturing (AM), also known as 3D printing, is a quickly evolving manufacturing technology that has changed the way goods are designed, developed, and manufactured [1]. AM has transformed conventional manufacturing processes by enabling the creation of complex geometries and customized products, reducing build times, and delivering substantial cost savings across a wide range of industries. [2]

The AM method includes the layering of material to create three-dimensional things. Unlike traditional manufacturing techniques, additive manufacturing allows for the production of components with complex forms and dimensions that would be difficult or prohibitively expensive to produce using traditional methods [4]. AM is a versatile technology that can be applied to a wide range of materials, including plastics, metals, ceramics, and composites, making it a popular manufacturing option for a variety of applications [5]. Despite having the potential for large-scale printing, AM is nevertheless constrained since the process parameters chosen affect the component quality and mechanical characteristics of an additively made item [6]. The selection of process parameters is crucial for 3D printed constructions because of the anisotropic behavior and sensitivity to it [7]. It's critical to determine which process variables are crucial for an AM approach out of all possible options. When these parameters are chosen correctly, higher mechanical characteristics and component quality can follow, whereas when they are chosen incorrectly, mechanical strength and quality might suffer [8]. As a result, process variable optimization becomes paramount significance. 3D printed items with the appropriate characteristics may be created by combining process factors in the ideal way. The additive manufacturing industry has evolved quickly in recent years, due to substantial investments in research and development that have resulted in continuous improvements in AM technology, materials, and procedures [9]. The advantages of additive manufacturing can be seen in a variety of sectors, including aircraft, medical, automobile, and consumer products [10]. This thesis will provide an in-depth examination of the additive manufacturing process, its various applications, and the impact of AM on traditional manufacturing methods. The thesis also seeks to investigate the challenges and constraints of AM, as well as to provide insights into future advances and advancements in this area. Overall, the goal of this study is to provide a comprehensive overview of additive manufacturing technology and its effect on modern production practices.

1.1 Fused Deposition Modelling

Out of the various AM techniques, FDM is one of the most popular and commonly used technique [11]. FDM was made commercially available in the initial 1990s, after the FDM technique was patented by the co-founder of Stratasys, Scott Crump, in 1989 [12]. In the FDM process, a continuous supply of thermoplastic filament via a spool is utilized for printing layers of material to build the part [13]. After an uninterrupted supply of material filament is available, it is heated to a semi-liquid phase by the heating element inside the liquefying head and this semi-liquid thermoplastic is extruded through the extrusion nozzle on the printing bed/ platform. The main working principle of FDM is that the semi-liquid thermoplastic filament materials do not solidify immediately when it extruded from nozzle on the printing platform, rather these semi-liquid thermoplastics for a-particular layer under construction fuse together, before curing/ solidifying into a layer-wise stacked part in surrounding ambient temperature [14]. The simplicity of the process, high-speed printing, and low cost are the main benefits of FDM [15]. Whereas, the disadvantages of FDM technique are process parameter-dependent mechanical properties (or anisotropic mechanical properties), poor surface finishing, layer-wise appearance of part and FDM printing materials limited to thermoplastic polymers only because thermoplasticity is the essential property for a material to be 3D printed through FDM technique [16]. Since the quality and mechanical characteristics of FDM printed parts essentially depend upon the proper (or optimal selection) of process parameters. Hence, to make FDM suitable for mass-production and more acceptable by industries, finding the optimal process parameters combination to improve the part quality and mechanical properties becomes of utmost importance. Fused Deposition Modeling (FDM) is a popular 3D printing technique that uses a thermoplastic filament to create objects layer by layer. Here are some benefits of FDM:

- **Versatility:** FDM can be used with a wide variety of materials, including ABS, PLA, nylon, and more. This makes it a versatile printing method for different applications [17].
- **Cost-effective:** FDM printers are generally more affordable compared to other 3D printing technologies, making them accessible to individuals and small businesses [18].
- **User-friendly:** FDM printing is relatively easy to use and does not require extensive training or expertise. This means that beginners can quickly learn how to use the technology [19].
- **High accuracy:** FDM printers are capable of producing parts with high [20].

While Fused Deposition Modelling (FDM) has many benefits, it also has some limitations and issues:

- **Surface finish:** Parts printed with FDM may have a rough surface finish due to the layer-by-layer printing process. This can be improved by post-processing techniques such as sanding or polishing [21].
- **Limited resolution:** FDM printers have a limited resolution, which can result in visible layer lines and reduced detail in the printed parts [22].
- **Support structures:** FDM parts with overhangs or complex geometries require support structures that must be removed after printing. This can be time-consuming and may result in damage to the part [23].
- **Warping:** Some materials used in FDM printing, such as ABS, can warp as they cool, causing the part to deform or detach from the build plate [24].
- **Material limitations:** FDM is limited to printing with certain types of materials, typically thermoplastics, which may not be suitable for all applications [25].
- **Limited strength:** While FDM parts can be durable, they may not have the same strength as parts made with other manufacturing techniques such as injection molding [26].
- **Environmental impact:** FDM printing requires a significant amount of energy and produces waste in the form of support structures and failed prints, which can contribute to environmental issues [27].

Overall, while FDM is a useful technology, it has limitations and issues that should be considered when selecting a 3D printing method for a particular application.

1.2 Critical 3D printing parameters in FDM

Fused Deposition Modelling (FDM) is a popular 3D printing technology that uses a thermoplastic filament to create objects layer by layer. The following are critical 3D printing parameters in FDM that affect the quality and accuracy of the printed part:

1. **Layer height:** This parameter determines the thickness of each layer printed. A smaller layer height results in a smoother surface finish and higher accuracy but increases the printing time [28].
2. **Printing speed:** The speed at which the printer moves the nozzle affects the quality of the print. Printing too fast can cause the material to smear or not adhere to the previous layer,

while printing too slowly can result in overheating and deformation of the part [29].

3. **Extrusion temperature:** This parameter determines the temperature at which the thermoplastic filament is melted and extruded. It affects the quality of the print by influencing the material flow and adhesion to the build platform [30].
4. **Bed temperature:** The temperature of the build platform affects the adhesion of the printed part to the build surface. A heated bed is recommended to prevent warping and detachment of the part during printing [31].
5. **Filament type:** The type and quality of the filament used can affect the quality of the print, including its strength, durability, and surface finish [31] [32].
6. **Infill density:** This parameter determines the density of the internal structure of the printed part. A higher infill density results in a stronger and more durable part but increases printing time and material usage [33].
7. **Support structures:** Overhangs and complex geometries require support structures to prevent the part from collapsing during printing. Support structures can affect the surface finish and require post-processing to remove [34].

Optimizing these parameters for a specific part can improve the quality and accuracy of the printed part and reduce waste and production time.

1.3 Effects of FDM Parameters on Part Quality:

The various parameters used in Fused Deposition Modelling (FDM) can have a significant impact on the quality of the printed part. Here are some effects of different parameters on part quality:

1. **Layer height:** The layer height can affect the surface finish of the part. A smaller layer height can produce a smoother surface finish but can increase printing time.
2. **Printing speed:** The printing speed can affect the quality of the part by influencing the material flow and adhesion to the previous layer. Printing too fast can result in material smearing or not adhering to the previous layer, while printing too slowly can result in overheating and deformation of the part.
3. **Extrusion temperature:** The extrusion temperature can affect the adhesion of the part to the build platform and the interlayer adhesion. An incorrect extrusion temperature can result in poor layer adhesion, which can cause the part to delaminate.

4. Bed temperature: The bed temperature can affect the adhesion of the part to the build platform. A heated bed can help prevent warping and detachment of the part during printing.
5. Filament type: The type and quality of the filament used can affect the strength, durability, and surface finish of the part. A high-quality filament can produce a smoother surface finish and stronger part.
6. Infill density: The infill density can affect the strength and weight of the part. A higher infill density can produce a stronger part, while a lower infill density can produce a lighter part.
7. Support structures: Support structures can affect the surface finish of the part and require post-processing to remove. Well-designed support structures can produce a smoother surface finish and prevent the part from collapsing during printing.

By optimizing these parameters, it is possible to produce high-quality 3D printed parts that meet the desired specifications. It is essential to understand the impact of each parameter and adjust them accordingly to produce the desired quality of the printed part. In the present article we have performed design of experiments (DoE) to short list the most effective build parameters among build speed, layer height, orientation, raster width and contour width. In DoE, the build time was set as the output parameters that would be affected by the chosen build parameters. In the later sections the quality and strength of 3D printed parts based on the short listed most effective build parameters were investigated.

CHAPTER 2: Material & Methodology

Acrylonitrile butadiene styrene (ABS) is widely used in material extrusion 3D printing. It is considered an ideal material for 3D printing, and its composition typically includes 15 to 35% acrylonitrile, 5 to 30% butadiene, and 40 to 60% styrene [35]. The study compared experimental results to the Technical Data Sheet provided by the manufacturer of Ultimaker ABS [36]. The properties of ABS is presented in Table 2.1.

Table 2.1: ABS Material data

Properties	Values	Units
Melting Point	225 - 245	°C
Tensile Stress at break	33.9	MPa
Flexural Strength	70.5	MPa
Elongation at break	4.8	%

Printing occurred on an Ultimaker 2 Extended+ 3D printer equipped with a 0.4 mm nozzle diameter. The 3D printed test specimens were produced in the XY plane using Ultimaker Cura 4.10.0, with three quality profiles: extra fine, fine, and normal. ABS filament with a diameter of 2.85mm was used, and a line infill pattern was employed during printing. The tests were conducted at an ambient temperature of $24\pm 2^\circ\text{C}$. Further details on the 3D printer specifications and fixed parameters can be found in the provided table 2.2.

Table 2.2: 3D Printer Specification & Fixed Parameters for Tensile & 3-Point bend test specimens

Fixed Printing Condition	Description
3D Printer Model	Ultimaker 2 Extended +
Printer Build Size	223mm x 223mm x 305mm
Material	ABS
Infill Density	100%
Raster angle	45° and 135°
Print Orientation	0° (flat on bed)
Support Structure	-
Rafts	Yes
Extruder Temperature	260 °C
Printing Bed Temperature	100 °C

The 3D printed ABS thermoplastic material specimens were subjected to mechanical tests to evaluate their mechanical properties.

2.1 Tensile Test

The tensile properties of the 3D printed specimens were evaluated following the widely recognized ASTM standard D-638. The shape and size of the specimens were based on the ASTM D-638, TYPE IV standards [37], as shown in figure 2.1

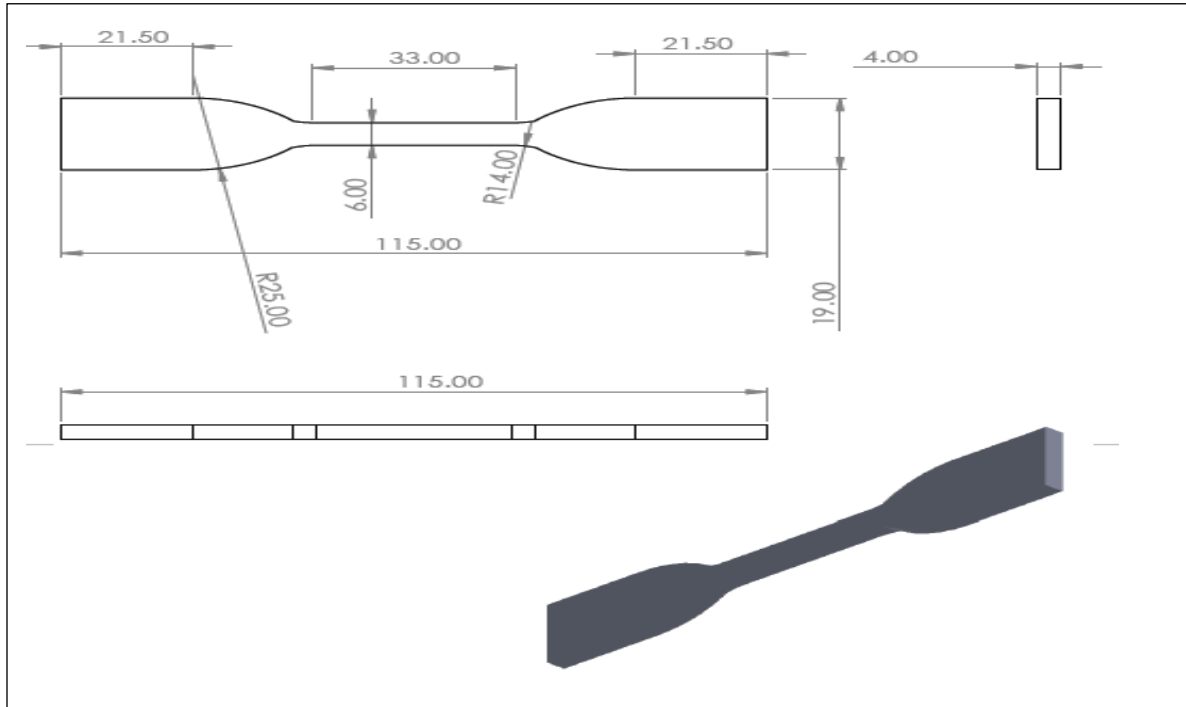


Figure 2.1: ASTM D-638 TYPE IV specimen drawing

Tensile testing was performed using a Haida HD-B607-S Universal Testing Machine, applying a testing speed of 5 mm/min and a load cell capacity of 50kN. The specimens were securely positioned in the UTM fixtures and subjected to a pulling force until failure occurred. The ultimate load at failure represented the maximum tensile strength of each specimen, indicating the maximum load it could withstand before breaking. Each sample consisted of three specimens, resulting in nine combinations examined to ensure a comprehensive evaluation of the mechanical performance of the 3D-printed parts across different printing parameters. Detailed parameters of the samples were presented in the table 2.3.

Table 2.3: Parameters of samples for Tensile & 3-Point bend test specimens

Sample	Layer Height (mm)	Print Speed (mm/s)
Sample 1	0.06	35
Sample 2	0.06	45
Sample 3	0.06	55
Sample 4	0.10	35
Sample 5	0.10	45
Sample 6	0.10	55
Sample 7	0.15	35
Sample 8	0.15	45
Sample 9	0.15	55

2.2 3-Point bending test

Three-point bending tests were conducted according to ASTM D790-10 [38],[39], as shown in figure 2.2, using a test fixture with 3 mm radius of loading nose and radii of the support noses. Bending measurements were taken using a Haida HD-B607-S universal testing machine, applying a strain rate of 1.5 mm/min and a 50kN load cell. The ASTM standard provides a standardized method to evaluate the flexural properties of materials, offering valuable insights into their stiffness and resistance to bending. Additionally, both tensile and flexural tests were performed on ABS blue and red specimens to comprehensively assess their mechanical properties.

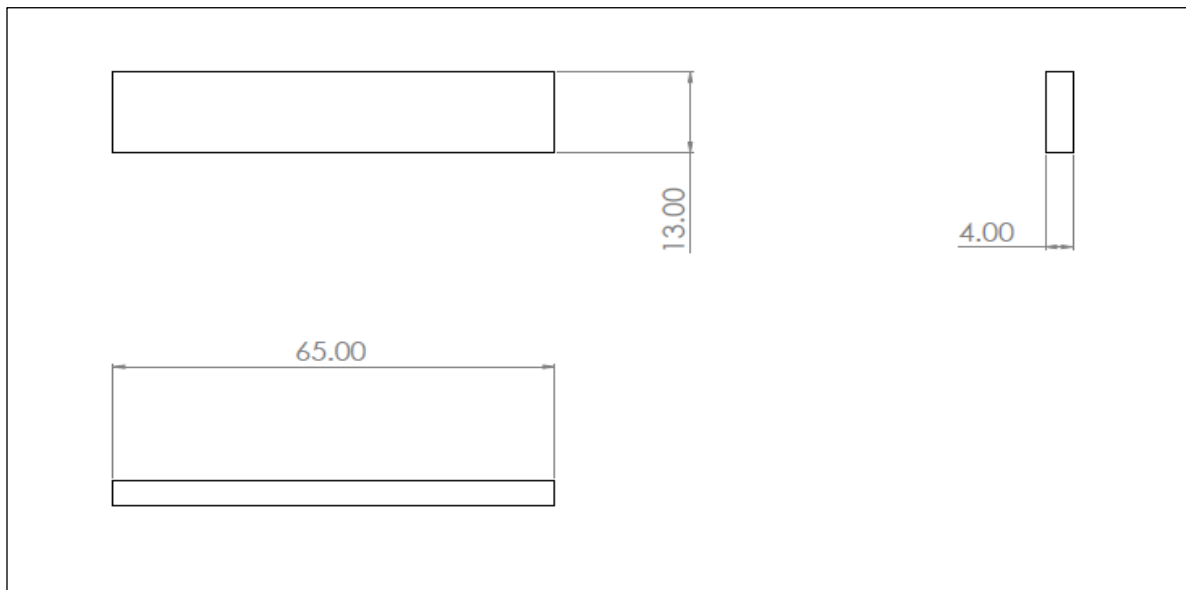


Figure 2.2: ASTM D790-10 specimen drawing

2.3 Artifacts 3D Scanning

A test artifact was utilized to evaluate the dimensional accuracy of 3D printed parts and assess the performance of the Ultimaker 2 Extended+ 3D printer. The artifact, provided by Gary Mac based on a NIST standard for additive manufacturing, was accompanied by engineering drawings and dimensions [40]. Two main factors identified by design of experiments technique, layer height (0.06 mm, 0.10 mm and 0.15 mm) and print speed (35 mm/s, 45 mm/s, and 55 mm/s), were considered, resulting in nine distinct combinations for evaluation. The design of the artifact took into account several crucial criteria, such as facilitating accurate measurements, incorporating various geometric features, minimizing printing time and material consumption, and eliminating the need for post-processing steps [41].

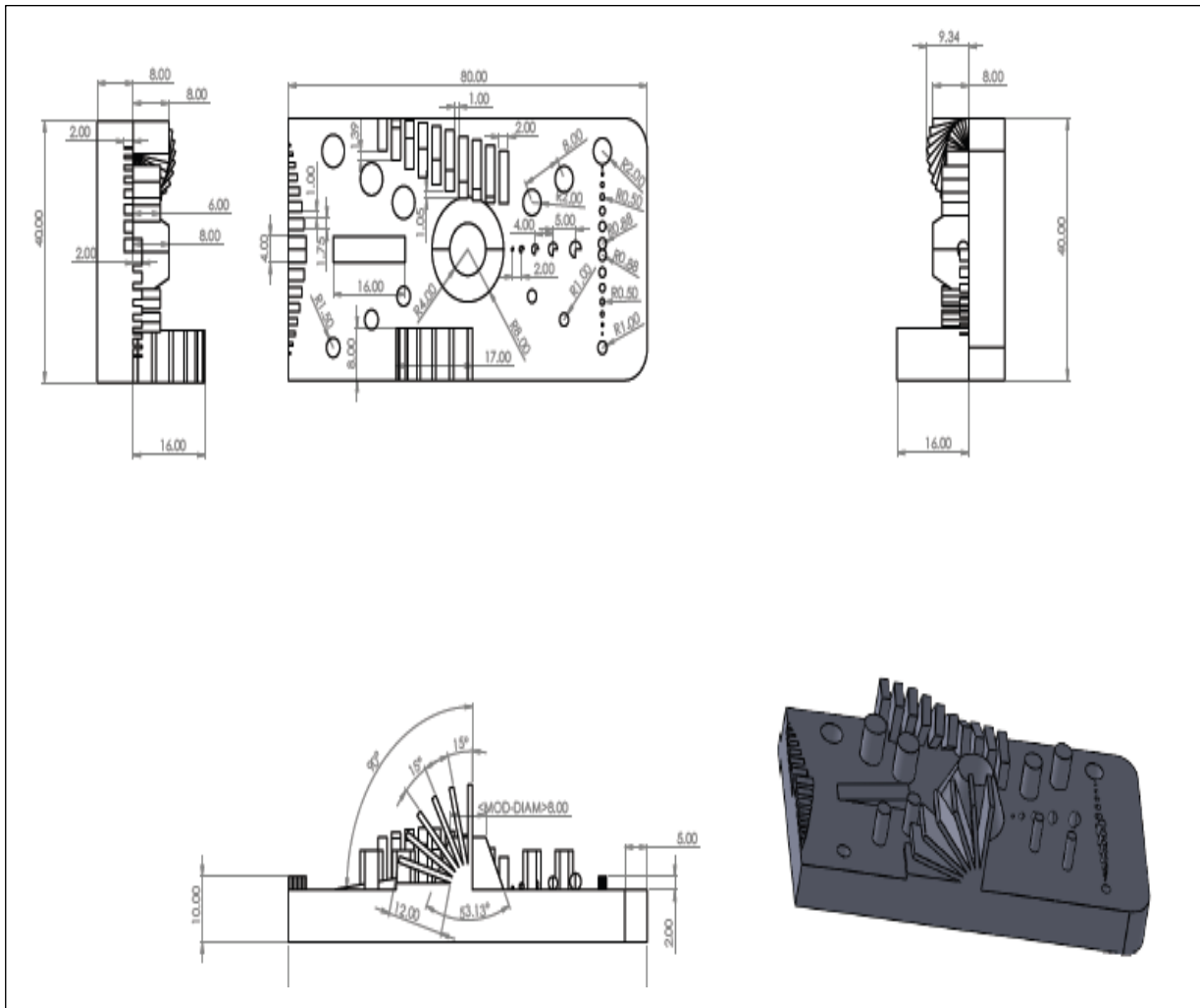


Figure 2.3: Test Artifacts Dimensions

The test artifact featured a rectangular base plate with specific dimensions (80 mm length, 40 mm width, and 8 mm thickness/height (Figure 2.3). It included different elements like circular pins and holes, rectangular pins and slots, a ramp, rectangular plates with varying angles, and a 270-degree revolving sphere ball, Figure 2.4 displays the names of the geometric features of the artifact. These elements served specific purposes in assessing the dimensional accuracy of printed parts. The circular pins and holes were used to evaluate the accuracy of circular diameter in the XY plane. The ramp features helped determine errors in the XY and Z axes, while the rectangular pins and slots were used to assess linear displacement errors in the XY plane. The sphere ball with a 270-degree revolve was employed to evaluate the printer's performance in printing balls of various diameters along the Z-axis.

To ensure precise evaluations, each printed part's dimensional accuracy was meticulously measured using a 3D scanner with **Handyscan 3D 700**. The 3D scanner used in this study has an accuracy 0.025mm. This data was then compared with the dimensions obtained from the CAD drawing by using the Geomagic Control X software. This research provided valuable insights into the capabilities and performance of the Ultimaker 2 Extended+ 3D printer when producing 3D printed parts with diverse geometries. The accurate measurements obtained from the 3D scanner allowed for a comprehensive evaluation of the printer's dimensional accuracy and the impact of different printing parameters on the final printed parts.

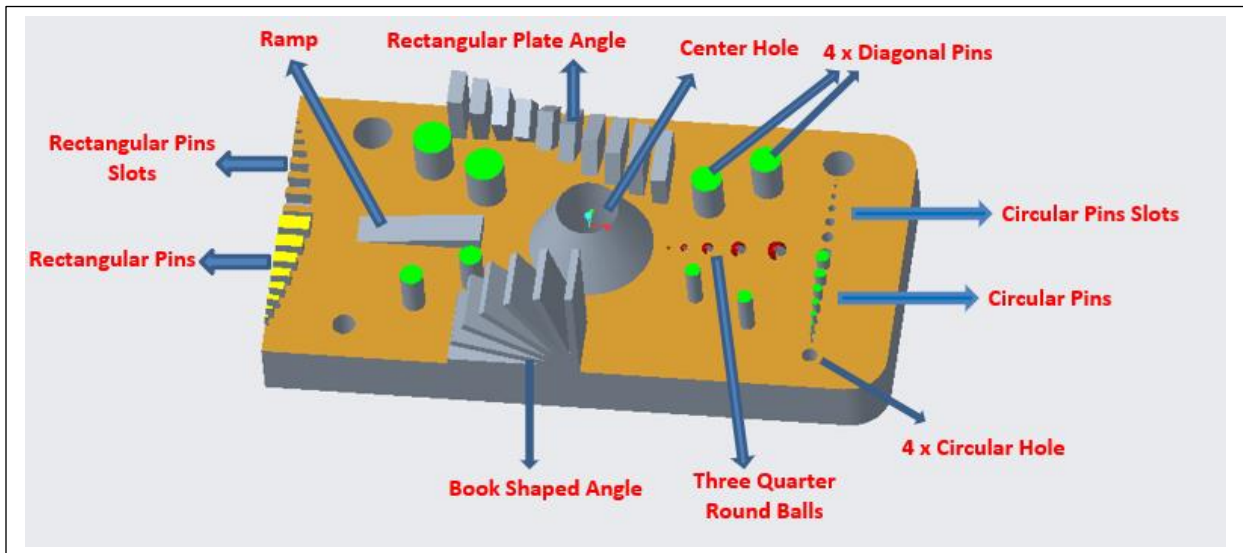


Figure 2.4: Test Artifact Geometries

2.4 Surface Roughness & Hatch Distance

The **Olympus DSX 1000 Digital microscope**, as shown in figure 2.5, was used for analysis of surface information. The DSX10-XLOB lens was utilized to analyze hatch distances of all the tensile and 3-point bending 3D printed parts. The microscope was set to capture images at a magnification of 20X/0.40, enabling a detailed examination of layer heights (0.06 mm, 0.1 mm, and 0.15 mm) and three print speeds (35 mm/s, 45 mm/s, and 55 mm/s). Consistently, hatch distance was evaluated within an area of 953x953 micrometers (μm) to ensure uniformity across all samples.

Surface roughness was measured by using **MarSurf M 310**, providing values for the selected image region. The roughness data Ra was calculated separately for both the top and side surface of the printed parts, offering comprehensive insight into the surface characteristics of the 3D-printed objects. Furthermore, the specimen with a layer height of 0.15 mm and a print speed of 45 mm/s was chosen for Acetone post-processing for 1.05 minutes to analyze surface roughness and assess its effectiveness in improving the part's finish. This analysis helped us assess the impact of various printing parameters on the surface quality of the printed parts.



Figure 2.5: Olympus DSX 1000 Digital microscope

CHAPTER 3: RESULTS & DISCUSSIONS

3.1 Design of Experiments (DoE)

3.1.1 Parameters Selection

Design of Experiment (DOE) serves as a valuable optimization tool to understand the role of process parameters and their impact on process outputs. By conducting multiple experiments, DOE allows us to determine the influence of various parameters on response variables. In this study, a full factorial DOE technique is employed, considering all possible combinations of factors and levels to comprehensively analyze main effects and interactions. The first step involves identifying the response factors to be optimized, followed by determining the parameters affecting these factors. In the evaluation of experimental results, the build time (R1) measured in minutes is selected as the response variable, as shown in Table 1. The research focused on examining the impact of build settings on process parameters, specifically the build time, by analyzing five parameters at designated levels (Table 2) to optimize the process and improve its efficiency. Using Design Expert 13 software and Full Factorial Design of experiments, factors such as layer height, print speed, orientation, contour width, and raster width will be analyzed. The main objective is to identify the most significant parameters for optimizing the 3D printing process. The identified significant parameters will then be further investigated to assess their influence on part quality and strength.

Table 3.1: Responses

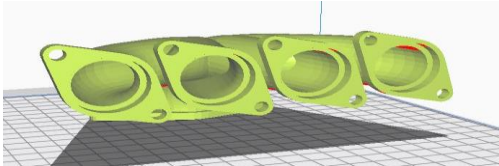
Response	Name	Units
R1	Build Time	minutes

Table 3.2: Selected Parameters

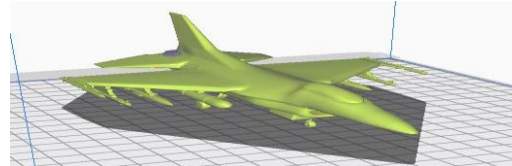
Parameter	Name	Units	Level	
			Minimum (-1)	Maximum (1)
A	Layer Height	mm	0.06	0.15
B	Print Speed	mm/s	35.00	55.00
C	Orientation	degree	0.00	90.00
D	Contour Width	mm	0.70	1.05
E	Raster Width	mm	0.20	0.40

3.1.2 Models

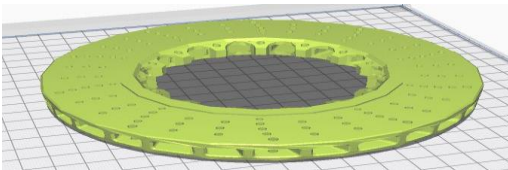
To assess the impact of the parameters, we performed the DOE technique using different models, including Exhaust Manifold, Airplane F 16, Disc, Table bowl, Battery AAA Base, Jig & Fixture, Main Chassis Combined, Blade 8, Arabic Motif, Groovi 3D Monster and Test Artifact designed using CAD software. The following figure 1 is shown below the DOE models.



Exhaust Manifold



Airplane F 16



Disc

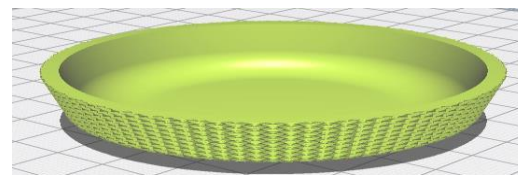
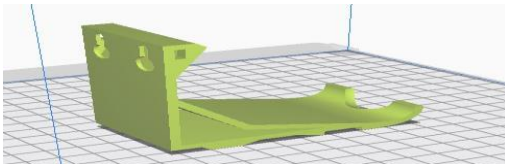
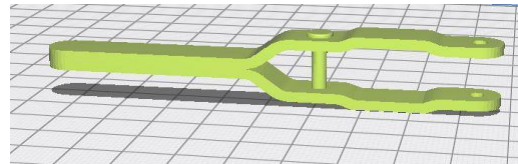


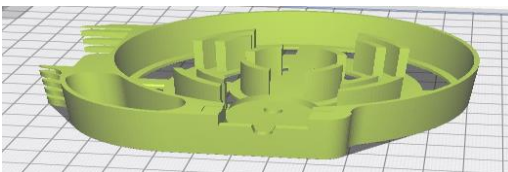
Table Bowl



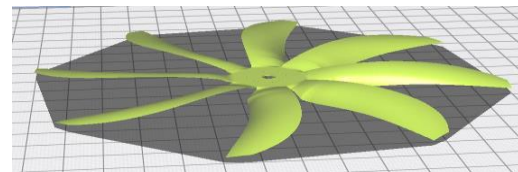
Battery AAA Base



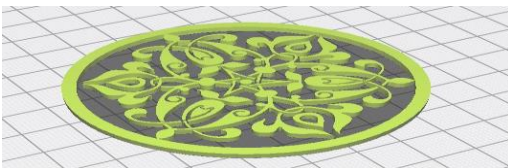
Jig & Fixture



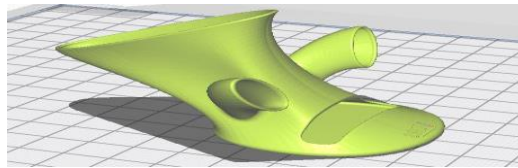
Main Chassis Combined



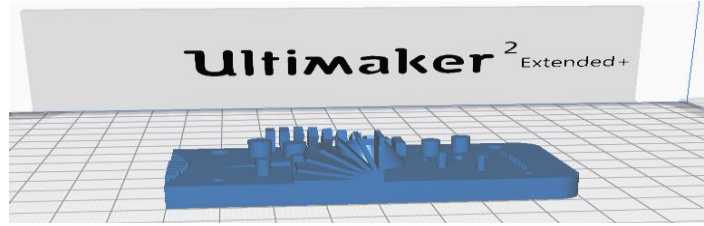
Blade 8



Arabic Motif



Groovi 3D Monster



Test Artifacts

Figure 3.1: DOE Models

3.1.3 Responses Measurements

To investigate how the build settings affect the process performance, this experimental research was focused on build time. The build time plays a crucial role in efficient and rapid prototype production. It is essential to optimize the build time by considering various parameters. To present the results here across the various models, the artifact model was chosen for the Design of Experiment (DOE) analysis. In the subsequent section, a detailed examination of the artifact model, including its dimensional accuracy and other relevant aspects, will be conducted. The goal was to evaluate the model and identify the main parameters contributing to the build time. A total of 33 runs were generated using Full Factorial Design with one centre point as a screening process. Design Expert 13.0 software was utilized for this analysis and Ultimaker Cura software was employed to calculate the values of response R1 for each combination of the models, which enabled the analysis of the responses. The specific values of R1 for each combination can be found in the provided table 3.

Table 3.3: Full Factorial 2⁵ DOE Experiments

Std	Run	Factor 1 A:Layer Height (mm)	Factor 2 B:Print Speed (mm/s)	Factor 3 C:Orientation (degree)	Factor 4 D:Contour Width (mm)	Factor 5 E:Raster Width (mm)	Response 1 Build Time (minutes)
1	19	-1	-1	-1	-1	-1	577
2	20	1	-1	-1	-1	-1	182
3	17	-1	1	-1	-1	-1	377
4	14	1	1	-1	-1	-1	132
5	23	-1	-1	1	-1	-1	671
6	28	1	-1	1	-1	-1	202
7	31	-1	1	1	-1	-1	423
8	24	1	1	1	-1	-1	151
9	13	-1	-1	-1	1	-1	607

10	32	1	-1	-1	1	-1	184
11	3	-1	1	-1	1	-1	397
12	30	1	1	-1	1	-1	133
13	22	-1	-1	1	1	-1	737
14	29	1	-1	1	1	-1	209
15	16	-1	1	1	1	-1	466
16	10	1	1	1	1	-1	156
17	6	-1	-1	-1	-1	1	555
18	9	1	-1	-1	-1	1	156
19	33	-1	1	-1	-1	1	363
20	27	1	1	-1	-1	1	113
21	7	-1	-1	1	-1	1	638
22	15	1	-1	1	-1	1	168
23	8	-1	1	1	-1	1	401
24	2	1	1	1	-1	1	125
25	26	-1	-1	-1	1	1	586
26	5	1	-1	-1	1	1	160
27	18	-1	1	-1	1	1	384
28	4	1	1	-1	1	1	116
29	1	-1	-1	1	1	1	706
30	11	1	-1	1	1	1	179
31	12	-1	1	1	1	1	444
32	25	1	1	1	1	1	132
33	21	0	0	0	0	0	305

3.1.4 Analysis of Variance (ANOVA) Results

Different combinations of five parameters were tested on various shaped models to obtain results for each combination. The collected data from these combinations underwent Analysis of Variance (ANOVA) to further analyze and interpret the results. For optimizing the build time, regression analysis was performed using Design Expert software, utilizing a linear regression model with a recommended square root transformation ($\lambda=0.5$) for this data. The accuracy of the regression models was validated through ANOVA, determining the statistical significance of the models based on probability values. The results of the ANOVA analysis are presented in Table 4.

Table 3.4: ANOVA table for Build time

Source	Sum of Squares	df	Mean Square	F-value	p-value	
Model	973.22	17	57.25	31493.38	< 0.0001	significant
A-Layer Height	835.08	1	835.08	4.59E+05	< 0.0001	
B-Print Speed	95.91	1	95.91	52761.5	< 0.0001	
C-Orientation	11.95	1	11.95	6576.04	< 0.0001	
D-Contour Width	2.27	1	2.27	1250.48	< 0.0001	
E-Raster Width	4.38	1	4.38	2410.02	< 0.0001	
AB	19.11	1	19.11	10513.63	< 0.0001	
AC	1.94	1	1.94	1066.41	< 0.0001	
AD	0.8947	1	0.8947	492.19	< 0.0001	
AE	0.5279	1	0.5279	290.42	< 0.0001	
BC	0.2787	1	0.2787	153.31	< 0.0001	
BD	0.0255	1	0.0255	14.05	0.0019	
BE	0.0242	1	0.0242	13.29	0.0024	
CD	0.2928	1	0.2928	161.06	< 0.0001	
CE	0.0795	1	0.0795	43.72	< 0.0001	
DE	0.0122	1	0.0122	6.69	0.0206	
ABC	0.3626	1	0.3626	199.45	< 0.0001	
ACD	0.075	1	0.075	41.28	< 0.0001	
Residual	0.0273	15	0.0018			

Based on the ANOVA results, a two-factor equation was developed for both coded and original factors to determine the relationship between the parameters and the responses. This equation helps in understanding the impact of the parameters on the build time and aids in optimizing the printing process. Regarding response R1 (build time in minutes), the coded equation is as follows:

$$\begin{aligned} \text{Sqrt}(\text{Build Time}) = & 17.55 - 5.11*A - 1.73*B + 0.6112*C + 0.2665*D - 0.37*E + \\ & 0.7728*A*B - 0.2461*A*C - 0.1672*A*D - 0.1284*A*E - 0.0933*B*C - 0.0283*B*D + \\ & 0.0275*B*E + 0.0957*C*D - 0.0498*C*E + 0.0195*D*E + 0.1064*A*B*C - \\ & 0.0484*A*C*D \end{aligned} \quad \text{Eq. (I)}$$

3.1.5 Significant parameters

The results obtained from applying the same technique or method on different models have shown that significant factors vary depending on the shape geometry of each model. This implies that different models have unique factors that significantly influence the response factors R1, and the contributions of these factors also vary among the different models. Therefore, it is crucial to consider the specific shape geometry and characteristics of each model when analyzing significant factors and their contributions to ensure accurate results. The provided table 5 presented and highlighting the distinctive relationship between the shape geometry and the influential factors for each model. By analyzing these specific factors and their contributions, it becomes possible to understand the individual characteristics and behavior of each model, facilitating more precise and customized optimization strategies based on the unique requirements of each model.

Table 3.5: Build Time Response Model & its Contributions

Part Name	Significant Models	Contributions %					Main Models
		A	B	C	D	E	
Exhaust Manifold	A, B, C, D, AB, AC, AD, BC, CD	57.9	30.7	8.9	0.6	-	A, B
F 16 Air plane	A, B, C, D, E, AB, AC, AE, BC, CD	62.5	36.3	0.8	0.09	0.1	A, B
Disc	A, B, C, D, AC, BC, CD	69	24.6	5.5	0.4	-	A, B
Table Bowl	A, B, C, D, E, AB, AC, AD, BC, BD, CD, ABC, ABD	46.6	23.6	21.1	0,5	0.04	A, B, C
Battery AAA Base	A, B, C, D, E, AB, AD, BC	66.7	29.7	2.1	0.03	0.1	A, B
Jig & Fixture	A, B, C, D, E, AC, AE, CD, CE, DE, CDE	69.7	25.8	2.1	0.6	0.4	A, B
Main Chassis Combined	A, B, C, D, AB, AC, AD, BC, ABC	45.5	25.4	20.8	0.2	-	A, B, C
Blade 8	A, B, C, AB, AC, BC	64.2	32.5	1.4	-	-	A, B
Arabic Motif	A, B, C, AB, AC, BC, CD	55	20.7	23.8	-	-	A, B, C
Groovi 3D Monster	A, B, C, BC	49.2	23.6	27	-	-	A, B, C
Test Artifact	A, B, C, D, E, AB, AC, AD, AE, BC, BD, BE, CD, CE, DE, ABC, ACD	85.8	9.9	1.2	0.2	0.5	A, B

The main model results from Table 5 indicate that **layer height** and **print speed** significantly influence build time. Consequently, further research will focus on investigating these two parameters' effects on part strength and quality to optimize 3D printed components for enhanced performance and reliability.

3.2 Test Artifact Results

3.2.1 Measured Values

In this section the table 3.6 provides feature measurements from 3D printed samples, giving a comprehensive overview of the dimensional accuracy and performance of the 3D printed parts.. Each specimen was independently 3D printed and measured, with the results for all layer heights and print speeds listed in the table 3.6. The average tolerance value of $\pm 0.1\text{mm}$ was used for 3D compare. In some cases, multiple measurements fell within the required tolerance range, but the closest values were highlighted in the blue box and shown in the optimum valued column, representing the most accurate results. The nominal values indicate the CAD model reference value for comparison.

Table 3.6: Artifacts Measured Values

All values in millimetres											
Description	Nominal Value	Measured Values									
		Layer Height (mm) - Print Speed (mm/s)									
		0.06-35	0.06-45	0.06-55	0.1-35	0.1-45	0.1-55	0.15-35	0.15-45	0.15-55	Optimum Value
Build Time											
Build Time (hours: minutes)		11:27	09:08	07:29	06:51	05:25	04:30	03:36	02:57	02:32	0.15-55 / 02:32
Boundary Dimensions											
Length	80.00	79.91	79.89	79.77	79.73	79.49	79.33	79.72	79.82	79.63	0.06-35 / 79.91
Width	40.00	39.92	39.64	39.51	39.59	39.57	39.53	39.76	39.69	39.66	0.06-35 / 39.92
Height (Thickness)	8.00	8.00	7.99	8.05	7.97	7.87	7.84	7.95	7.90	7.92	0.06-35 / 8.00
Round Corner Diameter	10.00	10.00	9.95	9.92	10.01	9.87	9.83	9.86	9.82	9.80	0.06-35 / 10.00
Centre Hole											
Inner Diameter	8.00	7.97	7.93	7.81	8.09	7.95	7.71	7.80	7.75	7.60	0.06-35 / 7.97
Height	8.00	7.88	7.81	7.82	7.63	7.53	7.48	7.69	7.52	7.53	0.06-35 / 7.88
Outer Diameter	16.00	16.04	16.01	15.90	15.88	16.08	15.93	16.06	16.09	15.95	0.06-45 / 16.01
Ramp											
Angle	7.13°	7.22°	7.26°	7.31°	7.32°	7.45°	7.39°	7.42°	7.19°	7.37°	0.15-45 / 7.19°
Length	16.00	15.97	15.95	15.92	15.89	15.80	15.60	15.35	15.17	15.16	0.06-35 / 15.97
Width	4.00	4.07	3.98	3.94	4.03	3.99	3.96	4.03	3.91	3.83	0.1-45 / 3.99
Height	2.00	2.06	1.98	2.00	1.99	2.04	2.06	1.96	1.92	1.95	0.06-55 / 2.00
Circular Hole											
Diameter A	2.00	1.69	1.61	1.60	1.65	1.53	1.43	1.50	1.43	1.32	0.06-35 / 1.69

Diameter B	3.00	2.95	2.79	2.73	2.94	2.84	2.60	2.58	2.58	2.62	0.06-35 / 2.95
Diameter C	4.00	3.96	3.85	3.78	3.91	3.88	3.68	3.74	3.60	3.56	0.06-35 / 3.96
Diameter D	5.00	4.97	4.93	4.84	5.04	4.95	4.71	4.72	4.66	4.67	0.06-35 / 4.97
Diagonal Pin											
Diameter E	2.00	2.02	1.95	1.89	1.91	1.85	1.81	1.87	1.76	1.71	0.06-35 / 2.02
Diameter F	3.00	2.98	2.96	2.91	2.90	2.86	2.84	2.85	2.76	2.73	0.06-35 / 2.98
Diameter G	4.00	3.95	4.04	3.92	3.91	3.86	3.81	3.90	3.84	3.78	0.06-45 / 4.04
Diameter H	5.00	4.98	4.94	4.90	4.92	4.87	4.81	4.91	4.84	4.79	0.06-35 / 4.98
Height	6	6.04	6.03	6.01	6.03	6.04	5.96	5.94	5.95	6.06	0.06-55 / 6.01
Rectangular Pin											
Width I	2.00	2.01	2.05	2.07	2.08	2.11	2.15	2.09	2.14	2.18	0.06-35 / 2.01
Width J	1.75	1.78	1.77	1.79	1.82	1.83	1.85	1.82	1.89	1.92	0.06-45 / 1.77
Width K	1.50	1.53	1.56	1.59	1.54	1.60	1.62	1.56	1.63	1.66	0.06-35 / 1.53
Width L	1.25	1.28	1.31	1.33	1.32	1.34	1.38	1.33	1.39	1.43	0.06-35 / 1.28
Width M	1.00	1.03	1.02	1.08	1.06	1.09	1.15	1.09	1.14	1.19	0.06-45 / 1.02
Width N	0.75	0.77	0.80	0.83	0.85	0.86	0.93	0.88	0.95	1.04	0.06-35 / 0.77
Width O	0.50	0.54	0.52	0.60	0.60	0.65	0.69	0.63	0.68	0.74	0.06-45 / 0.52
Width P	0.25	N/P	Not Printable								
Height	2.00	1.95	1.92	1.87	1.96	1.86	1.80	1.84	1.77	1.76	0.1-35 / 1.96
Rectangular Pin Slot											
Width I	2.00	2.00	2.02	1.96	1.98	1.96	1.92	1.96	1.94	1.91	0.06-35 / 2.00
Width J	1.75	1.76	1.80	1.78	1.77	1.80	1.84	1.79	1.83	1.87	0.06-35 / 1.76
Width K	1.50	1.54	1.51	1.47	1.46	1.42	1.38	1.44	1.39	1.34	0.06-45 / 1.51
Width L	1.25	1.22	1.18	1.15	1.17	1.15	1.09	1.15	1.12	1.07	0.06-35 / 1.22
Width M	1.00	0.97	0.94	0.98	0.95	0.91	0.85	0.93	0.88	0.82	0.06-55 / 0.98
Width N	0.75	0.72	0.66	0.64	0.65	0.60	0.56	0.61	0.58	0.53	0.06-35 / 0.72
Width O	0.50	0.46	0.47	0.44	0.45	0.41	0.37	0.42	0.38	0.35	0.06-45 / 0.47
Width P	0.25	N/P	Not Printable								
Depth	2.00	1.95	1.92	1.86	1.84	1.64	1.66	1.90	1.74	1.72	0.06-35 / 1.95
Circular Pin											
Diameter Q	1.75	1.73	1.69	1.64	1.61	1.59	1.50	1.67	1.66	1.61	0.06-35 / 1.73
Diameter R	1.50	1.47	1.48	1.41	1.43	1.42	1.39	1.43	1.41	1.38	0.06-45 / 1.48
Diameter S	1.25	1.24	1.29	1.32	1.27	1.30	1.34	1.30	1.35	1.38	0.06-35 / 1.24
Diameter T	1.00	0.99	1.03	1.02	1.06	1.08	1.11	1.05	1.13	1.16	0.06-35 / 0.99
Diameter U	0.75	0.79	0.81	0.80	0.77	0.86	0.91	0.82	0.90	0.96	0.10-35 / 0.77
Diameter V	0.50	0.55	0.58	0.60	0.58	0.60	0.65	0.63	0.67	0.69	0.06-35 / 0.55
Diameter W	0.25	N/P	Not Printable								
Height	2.00	1.98	1.93	1.88	1.94	1.87	1.85	1.95	1.86	1.82	0.06-35 / 1.98
Circular Pin Slot											
Diameter Q	1.75	1.73	1.71	1.74	1.69	1.60	1.57	1.63	1.61	1.56	0.06-55 / 1.74
Diameter R	1.50	1.43	1.39	1.37	1.39	1.37	1.34	1.38	1.31	1.27	0.06-35 / 1.43
Diameter S	1.25	1.27	1.26	1.31	1.21	1.18	1.14	1.23	1.18	1.12	0.06-45 / 1.26
Diameter T	1.00	1.02	1.05	1.07	1.03	1.06	1.11	1.05	1.14	1.19	0.06-35 / 1.02
Diameter U	0.75	0.77	0.82	0.85	0.87	0.90	0.93	0.86	0.95	0.97	0.06-35 / 0.77
Diameter V	0.50	N/P	Not Printable								
Diameter W	0.25	N/P	Not Printable								
Depth	2.00	1.92	1.88	1.82	1.86	1.84	1.74	1.85	1.77	1.73	0.06-35 / 1.92
Rectangular Plate Angle											
Width	5.00	4.91	4.84	4.64	4.63	4.65	4.72	4.82	4.78	4.72	0.06-35 / 4.91
Height	8.00	7.97	7.98	8.10	7.80	7.89	7.85	8.09	7.60	8.20	0.06-45 / 7.98
Thickness	2.00	2.00	1.97	2.10	2.06	2.09	2.15	2.12	2.18	2.23	0.06-35 / 2.00

Spacing between two rectangular Plates	1.00	0.94	0.96	0.91	0.94	0.85	0.81	0.86	0.82	0.78	0.06-45 / 0.96
Degree	10°	9.90°	9.58°	9.47°	9.59°	9.01°	8.93°	8.69°	8.53°	8.82°	0.06-35 / 9.90°
	20°	19.68°	19.72°	20.30°	19.37°	19.10°	19.12°	19.52°	19.13°	18.81°	0.06-55 / 20.30°
	30°	29.98°	29.88°	29.89°	29.80°	29.73°	29.63°	28.82°	28.77°	28.68°	0.06-35 / 29.98°
	40°	40.26°	39.97°	38.90°	39.59°	39.18°	38.52°	39.81°	39.61°	39.54°	0.06-45 / 39.97°
	50°	50.09°	50.28°	50.36°	50.08°	50.70°	50.61°	50.69°	51.53°	51.75°	0.10-35 / 50.08°
	60°	60.04°	60.10°	60.28°	60.24°	60.61°	60.82°	60.60°	61.05°	61.17°	0.06-35 / 60.04°
	70°	70.18°	70.33°	70.43°	70.39°	70.46°	71.48°	70.99°	71.28°	71.41°	0.06-35 / 70.18°
	80°	79.93°	79.69°	79.27°	79.90°	79.84°	79.76°	80.89°	79.70°	79.31°	0.06-35 / 79.93°
	90°	90.20°	90.71°	90.29°	90.84°	90.72°	91.16°	90.94°	91.02°	91.57°	0.06-35 / 90.20°
Book Shaped Angle											
Length	16.00	16.02	15.95	15.88	15.91	15.86	15.82	15.89	15.77	15.61	0.06-35 / 16.02
Thickness	1.00	1.03	0.98	0.95	0.96	0.93	0.92	0.94	0.93	0.90	0.06-45 / 0.98
Width	8.00	7.99	7.95	7.77	7.83	7.72	7.71	7.84	7.85	7.75	0.06-35 / 7.99
Angle Degree	15°	15.10°	14.86°	14.82°	14.73°	14.45°	13.92°	14.37°	13.81°	13.74°	0.06-35 / 15.10°
	30°	29.98°	30.13°	30.24°	30.29°	30.72°	30.91°	30.58°	30.89°	31.04°	0.06-35 / 29.98°
	45°	45.65°	45.42°	45.24°	45.40°	45.69°	45.85°	45.56°	46.04°	46.31°	0.06-55 / 45.24°
	60°	60.01°	60.04°	60.36°	60.46°	60.58°	60.72°	60.10°	61.04°	61.46°	0.06-35 / 60.01°
	75°	75.65°	75.19°	74.93°	75.11°	75.57°	75.63°	75.36°	76.28°	76.57°	0.06-45 / 75.19°
	90°	90.34°	90.67°	90.88°	90.60°	90.94°	91.23°	90.97°	91.28°	91.63°	0.06-35 / 90.30°
Three Quarter Round Ball											
Round Ball Diameter	0.50	0.70	0.74	0.80	N/P	N/P	N/P	N/P	N/P	N/P	0.06-35 / 0.70
	1.00	1.06	1.03	1.07	1.05	1.10	1.17	1.17	1.21	1.26	0.06-45 / 1.03
	1.50	1.45	1.44	1.41	1.43	1.42	1.30	1.31	1.28	1.22	0.06-35 / 1.45
	2.00	1.89	1.87	1.83	1.91	1.83	1.78	1.85	1.79	1.69	0.10-35 / 1.91
	2.50	2.39	2.44	2.52	2.42	2.33	2.23	2.35	2.31	2.26	0.06-55 / 2.52

3.2.2 3D Compare

The results demonstrate the impact of varying layer heights and print speeds on the dimensional accuracy of 3D printed parts. Careful analysis of the measurements helps identify parts that closely adhere to required tolerances, enabling manufacturers to optimize printing parameters for enhanced precision. The test artifact's diverse geometric features facilitate a comprehensive assessment of the 3D printing process's accuracy and capabilities, offering valuable insights for process optimization. Table 3.7 displays a deviation map, using green to indicate measurements within the acceptable tolerance range ($\pm 0.1\text{mm}$) and blue or red for measurements outside this tolerance, visually illustrating differences from the target values. The Table 3.8 illustrates the 3D compare results, with the peak (highlighted in a red box) representing values within the tolerance range, while the left and right sides show under-tolerance and over tolerance values, respectively. The table 3.9 displays all the 3D compare minimum, maximum, average, standard deviations, and tolerance values for all six combinations of layer height and print speed.

Table 3.7: 3D Deviation Map

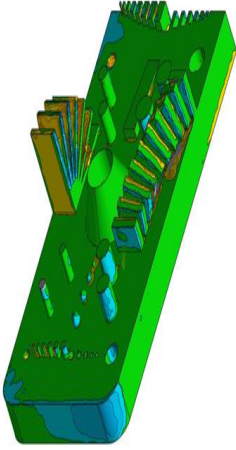
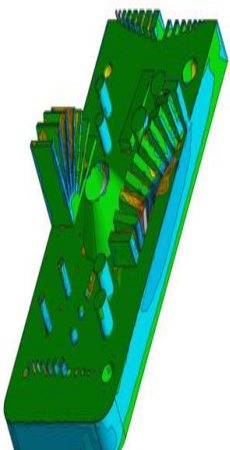
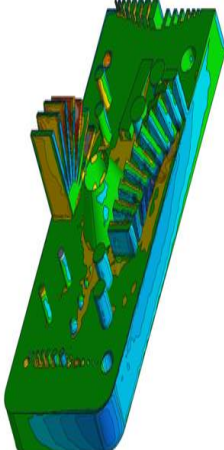
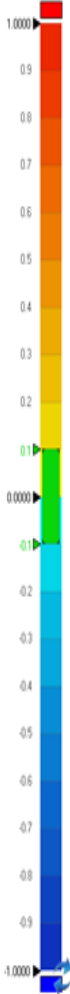
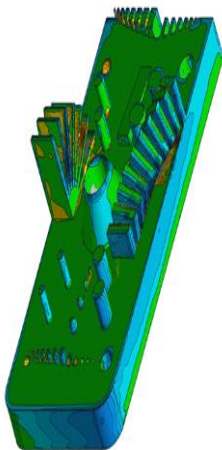
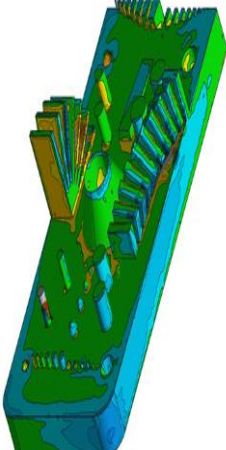
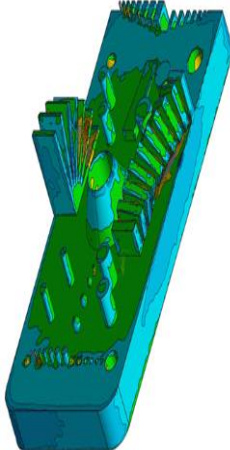
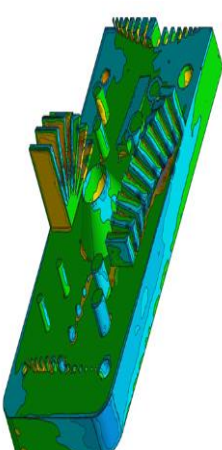
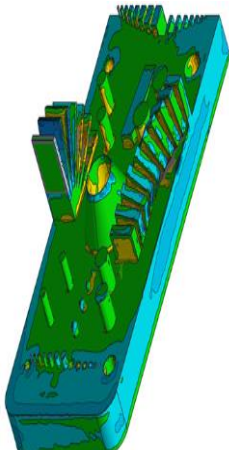
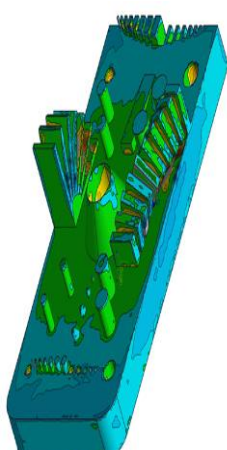
Layer Height (mm)	Print Speed (mm/s)			
	35	45	55	
0.06				
0.10				
0.15				

Table 3.8: 3D Compare Peak Tolerances

Layer Height (mm)	Print Speed (mm/s)		
	35	45	55
0.06			
0.10			
0.15			

Table 3.9: 3D Compare Tolerances Values

Description	Layer Height (mm) - Print Speed (mm/s)								
	0.06 - 35	0.06 - 45	0.06 - 55	0.1 - 35	0.1 - 45	0.1 - 55	0.15 - 35	0.15 - 45	0.15 - 55
Min.	-0.697	-0.831	-1.117	-1.124	-0.984	-0.964	-1.000	-1.042	-1.094
Max.	0.699	0.833	1.117	1.124	0.985	0.965	1.001	1.044	1.095
Avg.	0.004	-0.026	0.000	-0.059	-0.029	-0.090	-0.031	-0.033	-0.081
RMS	0.112	0.126	0.193	0.188	0.160	0.161	0.164	0.163	0.177
Std. Dev.	0.112	0.123	0.193	0.178	0.157	0.133	0.161	0.160	0.157
Var.	0.012	0.015	0.037	0.032	0.025	0.018	0.026	0.025	0.025
+Avg.	0.083	0.071	0.090	0.093	0.111	0.111	0.134	0.123	0.151
-Avg.	-0.068	-0.082	-0.197	-0.123	-0.113	-0.125	-0.101	-0.106	-0.132
In Tol.(%)	79.320	73.556	62.874	66.401	59.397	47.016	63.344	57.058	42.083
Out Tol.(%)	20.680	26.444	37.126	33.599	40.603	52.984	36.656	42.942	57.917
Over Tol.(%)	12.015	6.222	17.146	6.399	12.487	4.001	11.312	10.935	8.165
Under Tol.(%)	8.666	20.222	19.979	27.200	28.116	48.984	25.344	32.007	49.752

3.2.3 Percentage Error

The build time decreases with an increase in layer height and print speed. With 400 layers printed in 0.06mm layer height, 159 layers printed in 0.1mm layer height and 238 layers in 0.15mm layer height, more layers result in more time taken for printing. Additionally, higher print speeds contribute to reducing the overall build time by increasing the rate of printing. The figures display the percentage error from the dimensions of the computer-aided design (CAD) model for the additive manufacturing test artifact. The percentage error between the measured dimensions of the printed samples and the reference model is calculated using Eq. (II).

$$\frac{\text{Measured Value} - \text{Nominal Value}}{\text{Nominal Value}} \times 100 \% \quad \text{Eq. (II)}$$

Figure 3.2 presents measurements of length, width, height, and round corner diameter of a printed specimen base plate's outer edge, with corresponding percentage errors relative to specified dimensions. Reference dimensions for the base plate are 80 mm (length), 40 mm (width), 8 mm (height), and 10 mm (round corner diameter). The graph indicates that increasing dimensional values correlate with reduced error percentages, for height, where decreasing values correspond to higher error percentages.

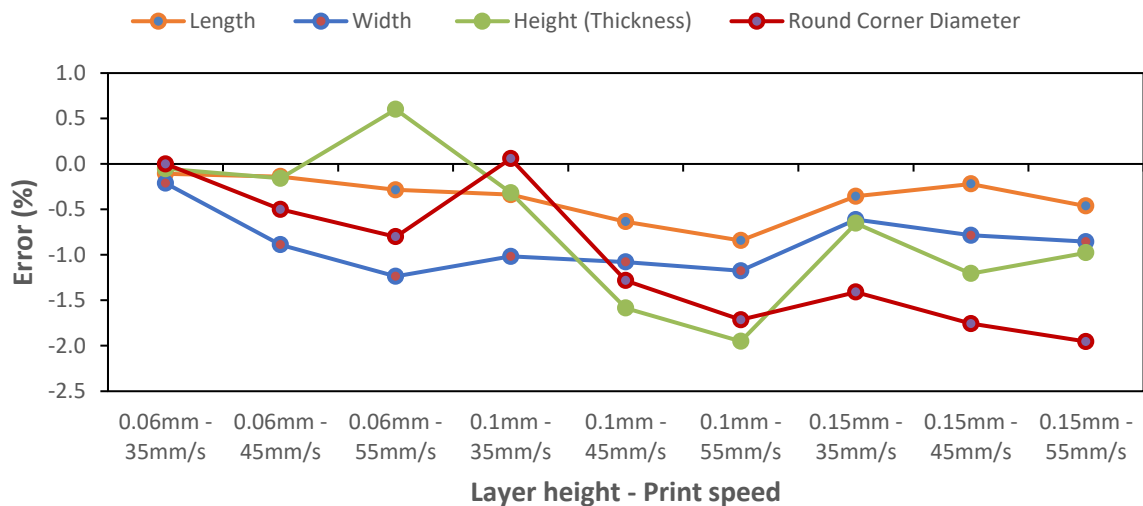


Figure 3.2: Boundary Dimensions Error % Deviation

In Figure 3.3, lateral features are depicted, featuring a centrally positioned circular hole within the specimen. The CAD model outlines dimensions of 8mm inner diameter, 16mm outer diameter, and 8mm height. The associated error percentage graph highlights the center hole's

optimal performance at a 0.06mm layer height. Negative percentages indicate measured values falling below the specified references, indicating a deviation from desired specifications.

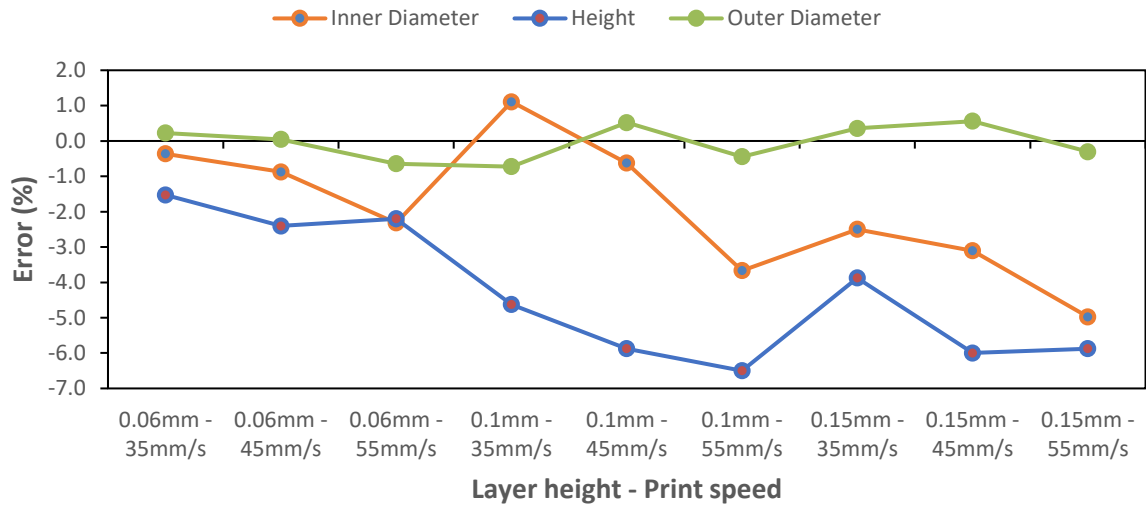


Figure 3.3: Centre hole Dimensions Error % Deviation

To assess the machine's capability in constructing openings along both horizontal and vertical directions, a ramp feature was introduced. In Figure 3.4, the depicted percentage error pertains to the ramp's dimensions, progressively increasing in height (2mm) and length (16mm). The reference specifications entail an angle of 7.13 degrees and a width of 4mm. A layer height of 0.06mm combined with a print speed of 45mm/s exhibits the minimal error percentage among ramp dimensions, indicating high accuracy in achieving the desired dimensions

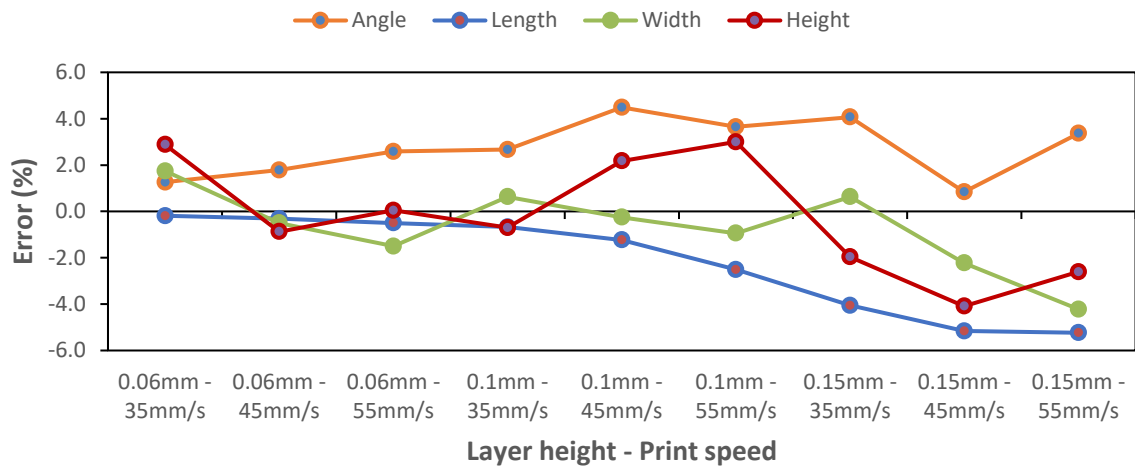


Figure 3.4: Ramp Dimensions Error % Deviation

Figure 3.5 displays the percentage error in circular hole dimensions, where reference values for diameter A, B, C, and D are 2mm, 3mm, 4mm, and 5mm, respectively. The results indicate that smaller diameters exhibit higher percentage errors, which decrease as the diameter increases, relative to the layer height. Among the circular hole dimensions, the combination of layer height 0.06mm and print speed 35mm/s exhibits the minimum error percentage, reflecting high accuracy in achieving the desired dimensions.

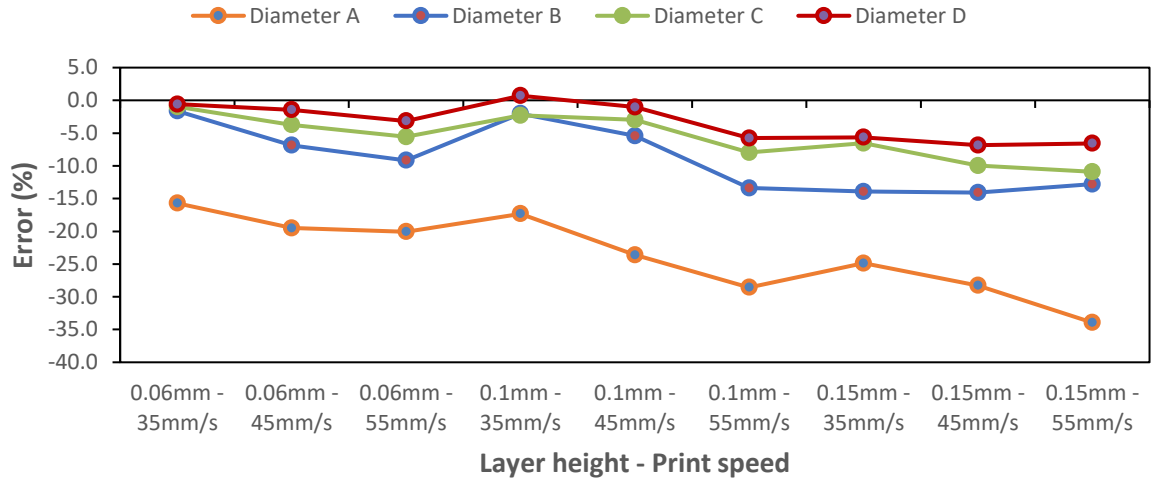


Figure 3.5: Circular Hole Error % Deviation

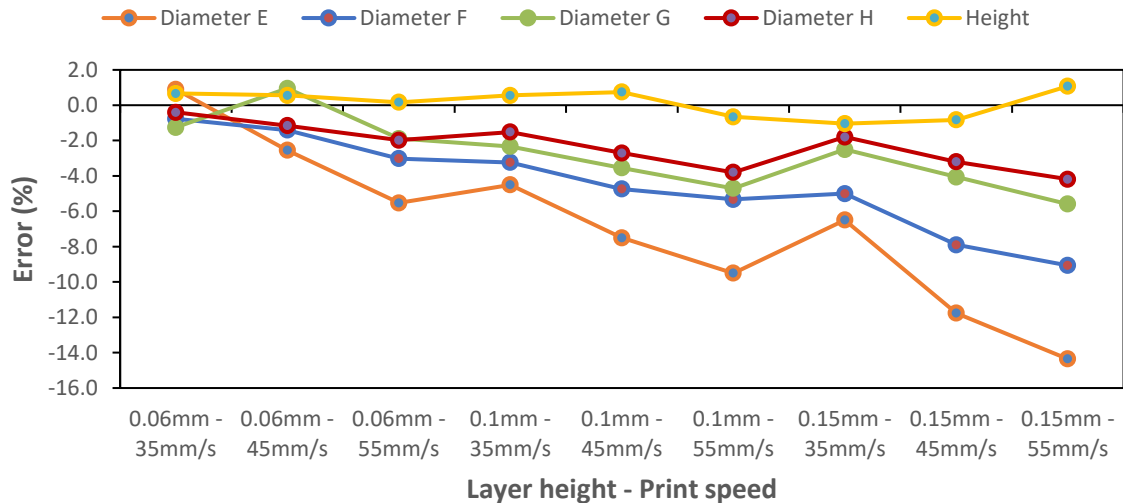


Figure 3.6: Diagonal Pins Dimensions Error % Deviation

In Figure 3.6, the percentage error for diagonal pin dimensions and heights is depicted. The data represents averages from two diagonal pins for each diameter, along with the mean height

from eight diagonal pins. Reference values for diameters E, F, G, and H are 2mm, 3mm, 4mm, and 5mm, respectively, with a constant 6mm height for all diagonal pins. These pins were utilized to assess circularity errors in both X and Y axes. Similar to the circular hole observations, smaller diameters exhibit higher error percentages, progressively diminishing with diameter increase. Notably, height dimensions in the z-axis plane display the least error percentage relative to layer height and print speed. Among the diagonal pin dimensions, the 0.06mm layer height coupled with print speeds of 35 and 45mm/s demonstrates the least error percentage, indicating exceptional accuracy in achieving intended dimensions.

The inclusion of rectangular pins aimed to assess the process's capacity to construct parallel thin-walled structures without additional supports. Figures 3.7 and 3.8 depict the percentage error in dimensions for both rectangular pins and slots. The pins represent the height above the rectangular base plate, while the slot denotes rectangular pins situated within the base plate. The results show the average of diagonal pins height and depth for all eight rectangular pins. Width dimensions I through P are specified as 2mm, 1.75mm, 1.5mm, 1.25mm, 1mm, 0.75mm, 0.5mm, and 0.25mm, respectively, with a common 2mm height and depth for both rectangular pins and slots. Results demonstrate that reducing width in both cases elevates the error percentage.

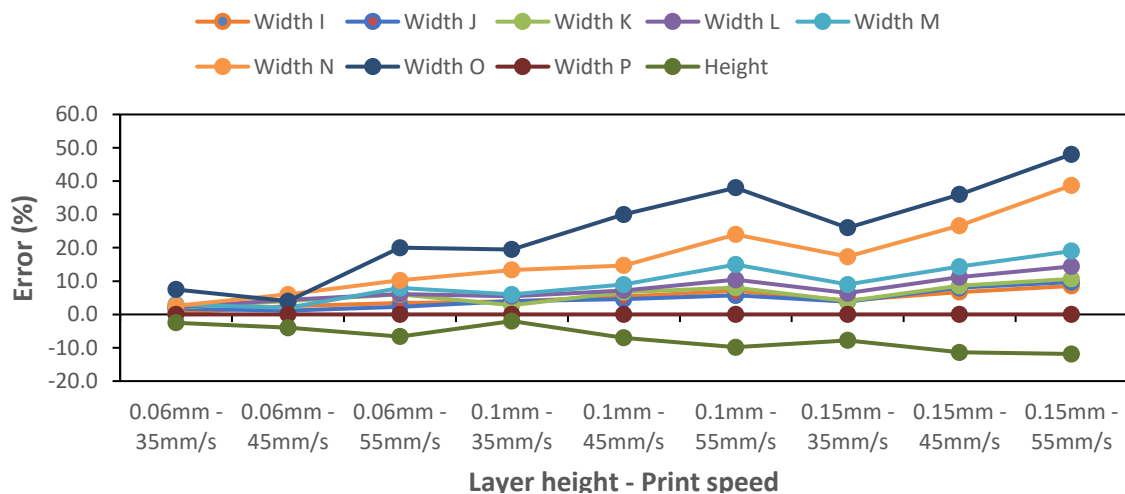


Figure 3.7: Rectangular Pins Dimensions Error % Deviation

However, limitations exist for specific width values. Width P (0.25mm) for rectangular pins and slots is not printable across all nine combinations of layer height and print speed, yielding a value of 0 (N/P) in Figures 3.7 and 3.8. This underscores the printer's constraint in handling slot features below 0.5mm. Rectangular pins exhibit widths equal to or greater than the reference,

whereas slot measurements fall below or match the reference. Notably, the rectangular pin and slot dimensions, the 0.06mm layer height combined with print speeds of 35 and 45mm/s shows minimal error percentages, indicating heightened precision within these settings.

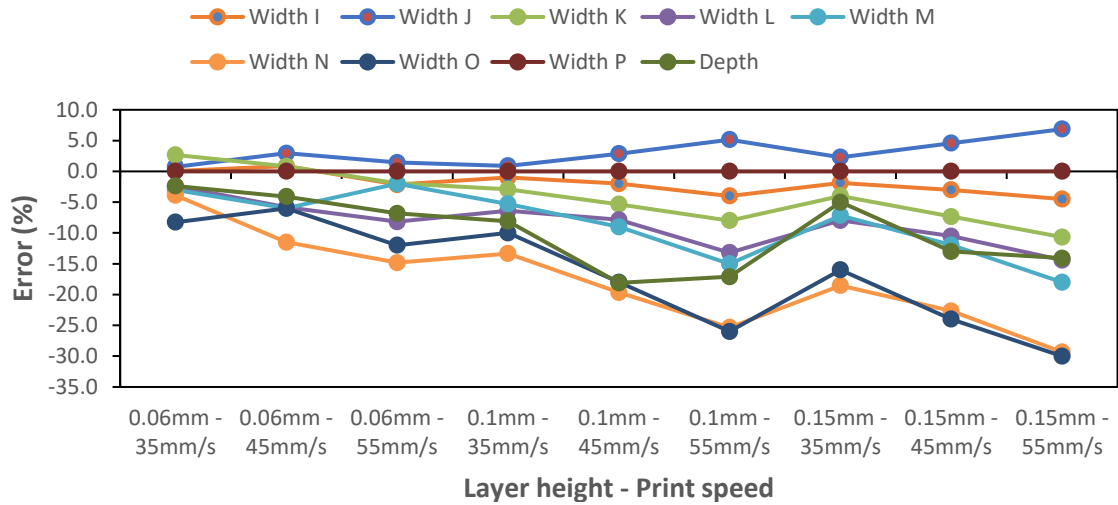


Figure 3.8: Rectangular Pins Slot Dimensions Error % Deviation

Figure 3.9 and 3.10 display the percentage error in circular pins and slots dimensions. These pins were designed to assess the process's capability to build thin structures. The results represent the average of height and depth for all seven circular pins. The reference values for circular pins Q, R, S, T, U, V, and W are 1.75mm, 1.5mm, 1.25mm, 1mm, 0.75mm, 0.5mm, and 0.25mm,

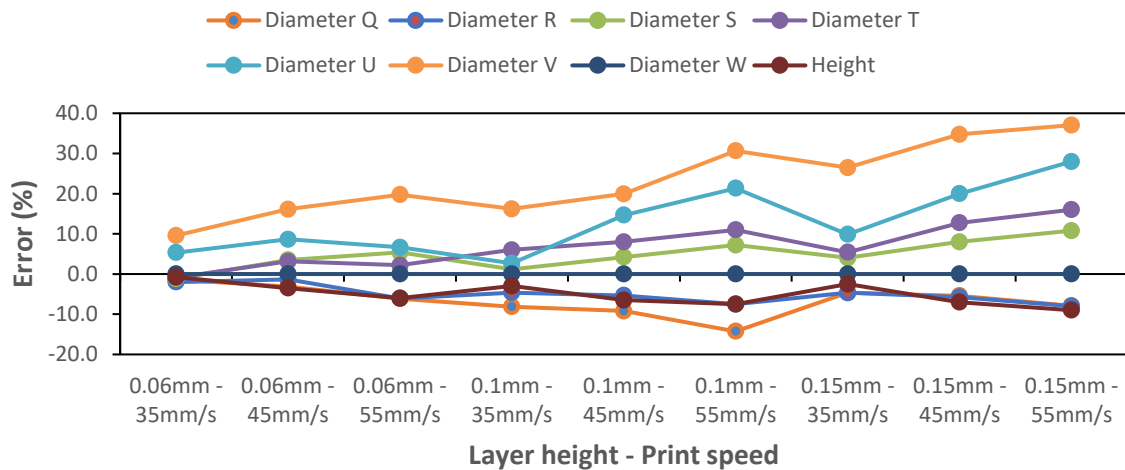


Figure 3.9: Circular Pins Dimensions Error % Deviation

respectively, with a height and depth of 2mm for the circular pins and slots. The circular pins exhibit similar trends for equivalent rectangular pins dimensions, showing consistent results across all measured diameters. However, diameter W with 0.25mm was not printable (N/P) among all 9 combinations. In the case of circular pin slots, diameters V and W with 0.5mm and 0.25mm were not printable (N/P). Among the circular pins and slot dimensions, the combination of layer height 0.06mm and print speed 35mm/s exhibits the minimum error percentage.

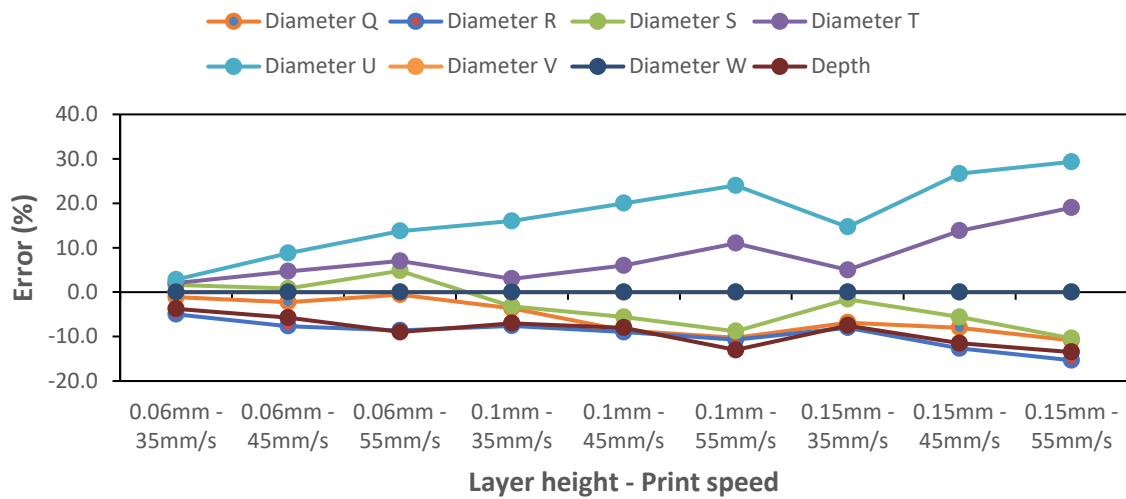


Figure 3.10: Circular Pins Slot Dimensions Error % Deviation.

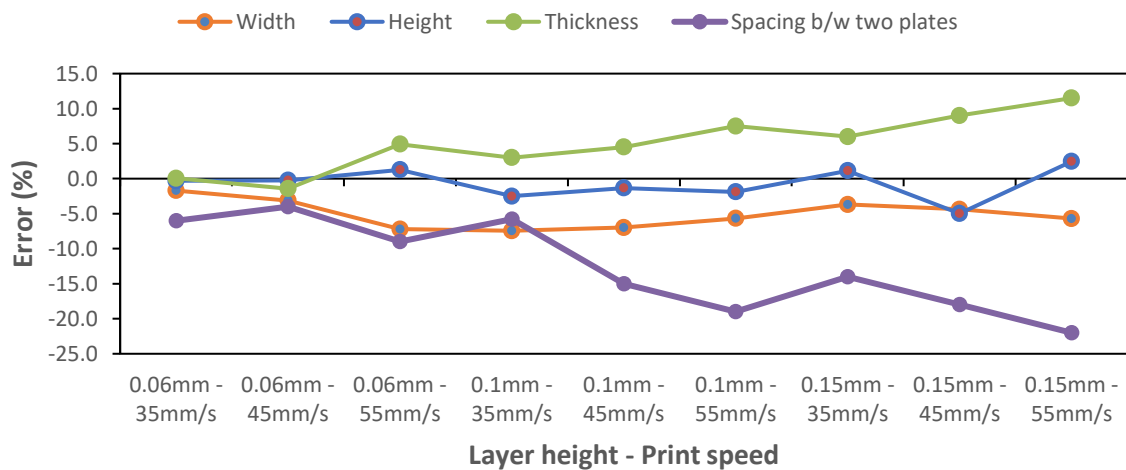


Figure 3.11: Rectangular plate Dimensions Error % Deviation

The percentage error for angle degrees in 3D printed dimensions was analyzed for both the rectangular plate and booked shape as shown in figure 3.11 to 3.13. The rectangular plate had

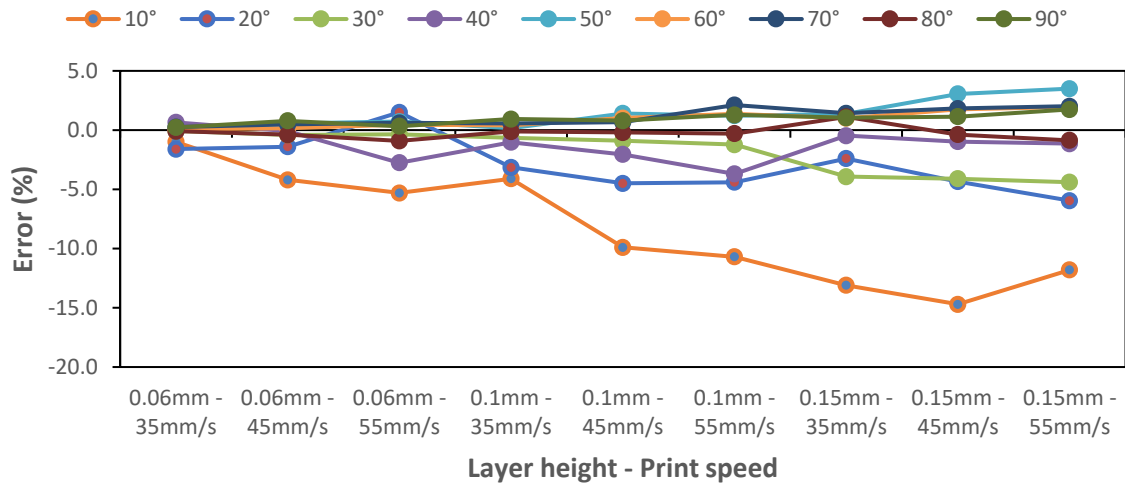


Figure 3.12: Rectangular plate Angle (degrees) Error % Deviation

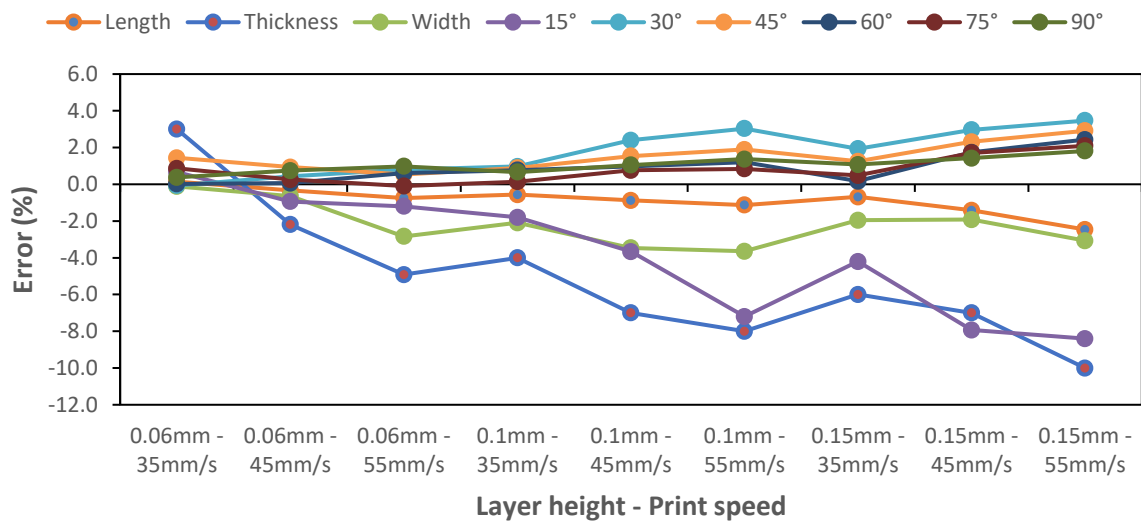


Figure 3.13: Book Shaped Dimension & Angle Error % Deviation

dimensions of 5mm width, 8mm height, and 2mm thickness, with a distance of 1mm between two plates and a 10-degree angle difference. Similarly, for the booked shape, the length, width, and thickness were 16mm, 8mm, and 1mm, respectively, with a 15-degree angle difference. Figures 3.11 to 3.13 demonstrate that as the angle increases from 0 to 90 degrees, the percentage error decreases in both cases. The error was more pronounced up to 50 degrees in the rectangular plate angle. Additionally, the horizontal distance between two rectangular plates showed a significant error percentage. In both cases, the combination of layer height 0.06mm and print speed 35 and 45mm/s demonstrated the minimum error percentage, indicating higher accuracy for these settings.

The three-quarter round ball diameter describes a ball rotated by 270 degrees and printed across diameters ranging from 0.50mm to 2.50mm. Figure 3.14 illustrates the percentage error, revealing that the 0.5mm diameter was only achievable at a 0.06mm layer height and all print speed combinations, while being not printable (N/P) with 0.10mm and 0.15mm layer heights at all print speeds. As ball diameter increases, the error percentage decreases. The combination of a 0.06 & 0.1mm layer height, and a print speed of 35mm/s demonstrated the least percentage error among all specimens of round ball diameters.

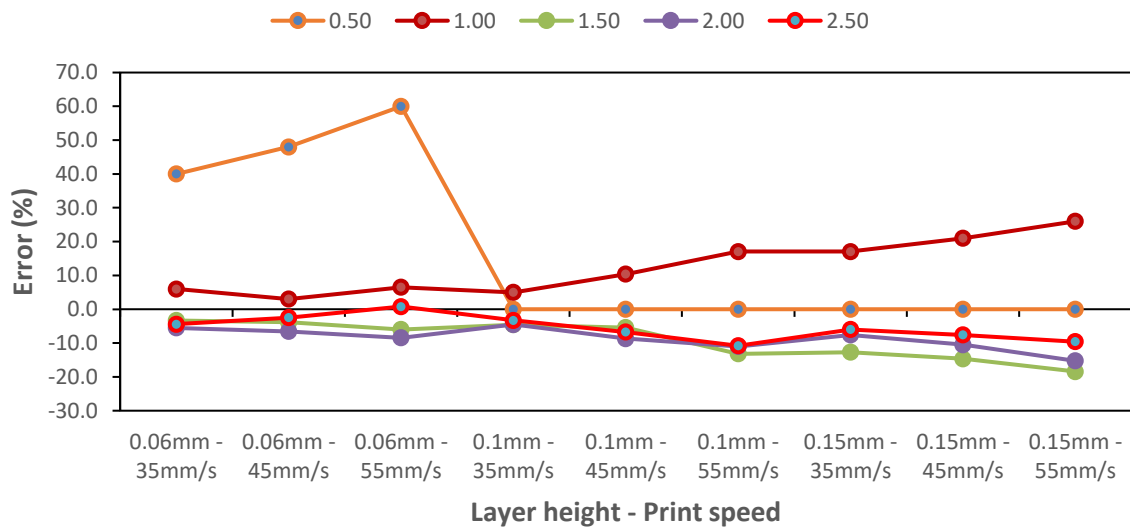


Figure 3.14: Round Ball Diameter Error % Deviation

3.3 Tensile Test ASTM D-638

After the 3D printing process, the mechanical properties of the samples were assessed and the table provides valuable insights into the mechanical properties of 3D-printed ABS with 100% infill, showing the relationship between layer height, print speed, and material strength. It demonstrates that higher print speeds generally result in weaker 3D-printed objects, as indicated by the decrease in Ultimate Tensile Strength (UTS) with increasing print speed. Conversely, extra fine layer height lead to stronger parts, with the maximum UTS observed at a layer height of 0.06 mm. Based on the data, the combination of a layer height of 0.06 mm and a print speed of 35 mm/s exhibits the highest overall strength, ductility, and strain at F max. It achieved the highest UTS value of 38.17 MPa, indicating maximum resistance to breaking. Conversely, a layer height of 0.15 mm and a print speed of 55 mm/s resulted in the lowest strength, ductility, and strain at F max. The

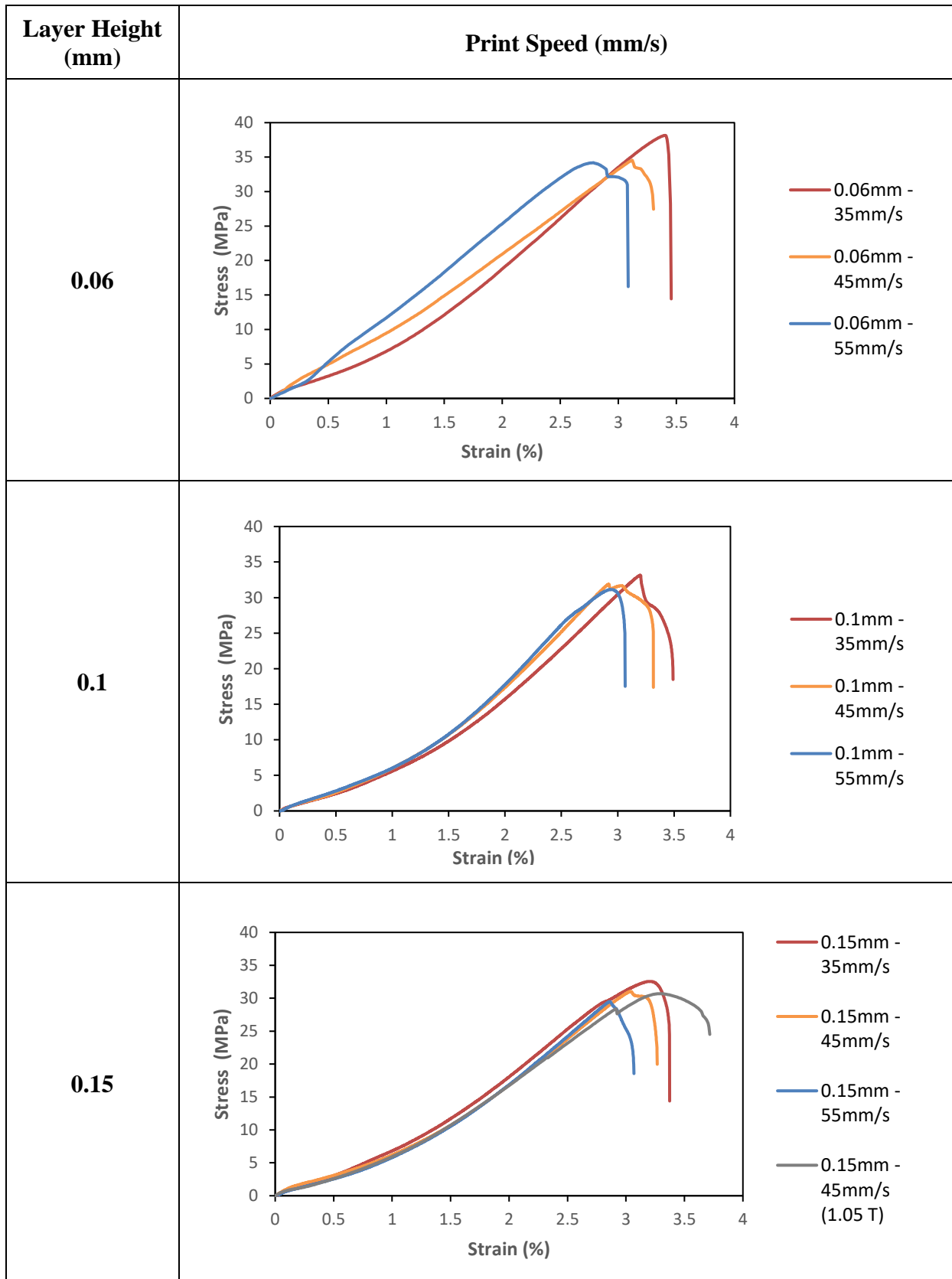
UTS value was reduced to 29.48 MPa, indicating weaker parts. The result revealed that acetone treatment had no significant effect on the tensile strength of ABS 3D printed parts. However, there were noticeable changes in strain percentage and maximum length, indicating improved ductility and elongation properties.

Table 3.7: Tensile Testing Experimental Data

Layer Height (mm)	Print Speed (mm/s)	F max (N)	UTS (MPa)	Length at Fmax (mm)	Length max (mm)	Strain (%)	Strain at F max (%)
0.06	35	916	38.17	3.92	3.97	3.45	3.40
0.06	45	829.2	34.55	3.59	3.80	3.30	3.12
0.06	55	820.4	34.18	3.20	3.55	3.09	2.78
0.1	35	795.6	33.15	3.68	4.01	3.49	3.20
0.1	45	765.2	31.88	3.36	3.82	3.31	3.03
0.1	55	747.4	31.14	3.38	3.53	3.07	2.94
0.15	35	781.2	32.55	3.68	3.88	3.37	3.20
0.15	45	744.6	31.03	3.49	3.76	3.27	3.04
0.15	55	707.5	29.48	3.29	3.53	3.07	2.86
0.15	45 (1.05T)	736.6	30.69	3.79	4.27	3.71	3.29

The Stress-Strain graph and table show varying ultimate tensile strengths for each layer height combination with three different print speeds. Among the print speeds, 35mm/s consistently exhibits the highest ultimate tensile strength. The Ultimate Tensile Strength graph reveals a decrease in UTS with higher layer heights and print speeds.

Table 3.8: Tensile Testing Stress Strain Graph



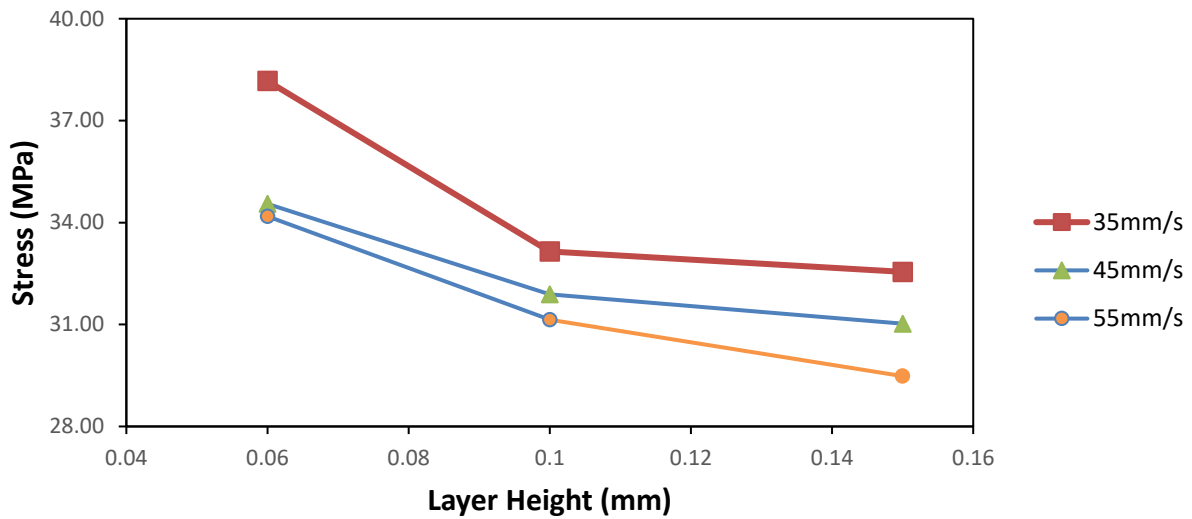


Figure 3.15: Ultimate Tensile Strength D 638 Graph

The graph illustrates a consistent elongation percentage across varying layer heights, with slight variations attributed to changes in print speed. The setting of 0.06mm layer height and 35mm/s print speed demonstrates ductility, reflected in a strain value of 3.45%, and also resilience at the point of failure, with a strain at F max reaching 3.4%. Notably, the 0.1mm layer height and 35mm/s print speed combination exhibits the highest elongation at 3.49%. In contrast, the 0.15mm layer height and 55mm/s print speed setup showcases the lowest elongation of 3.07%, implying limited plastic deformation capability before failure, as depicted in Figure 3.16.

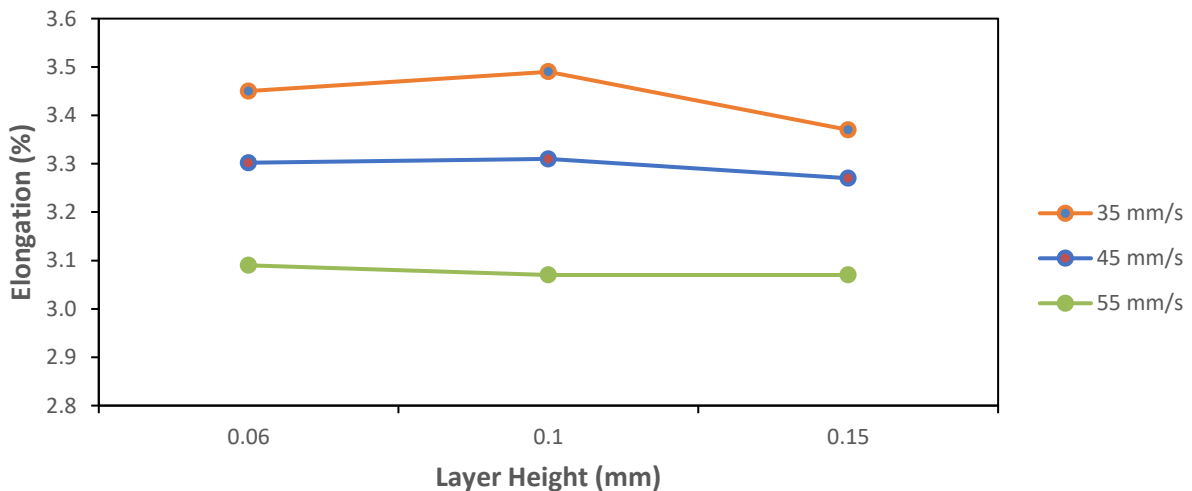


Figure 3.16: Tensile Testing Elongation (%) Graph

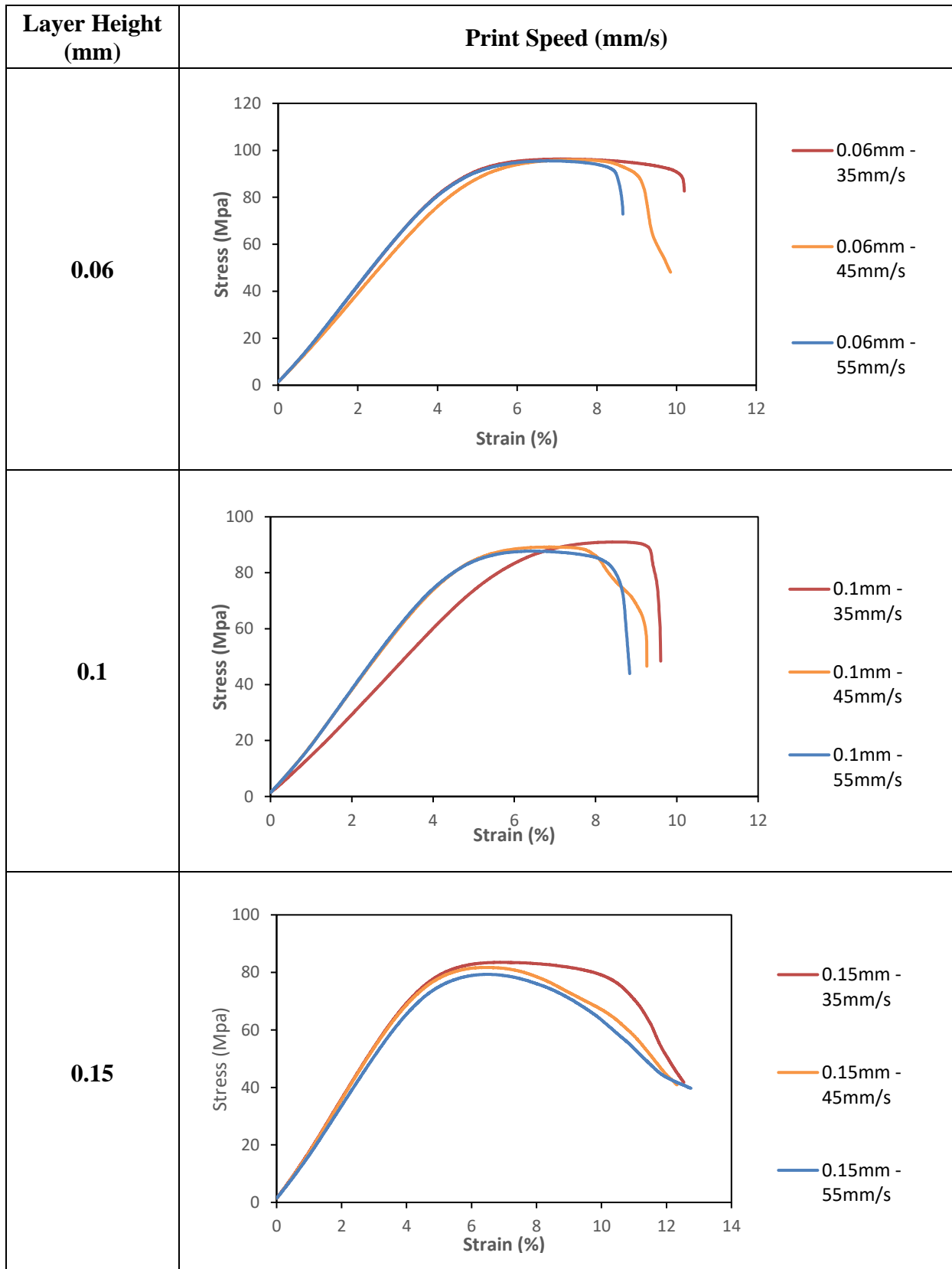
3.4 3-Point Bend Test ASTM D-790

Same as tensile testing the flexure strength values are shown for each combination of layer height and print speed. As expected, higher flexure strength values indicate greater resistance to bending before breaking. For example, the specimens printed with a layer height of 0.06 mm at a print speed of 35 mm/s had a flexure strength of 96.32 MPa, which was higher than the flexure strength of specimens printed with other combinations of layer height and print speed. Similar to tensile testing, flexural strength values indicate that higher values correspond to greater resistance to bending. The relationship between layer height and print speed with flexural strength is consistent with the findings from the tensile tests.

Table 3.9: 3-Point Bending D-790 Experimental Data

Layer Height	Print Speed	Fmax	Flexure Strength	Length at Fmax	Length max	Strain	Strain at F max
(mm)	(mm/s)	(N)	(MPa)	(mm)	(mm)	(%)	(%)
0.06	35	205.5	96.32	4.6	6.63	10.19	7.08
0.06	45	204.8	96.00	4.8276	6.404	9.849	6.99
0.06	55	203.8	95.54	4.4	5.62	8.65	6.77
0.1	35	194.2	91.02	5.46	6.24	9.602	8.46
0.1	45	190.3	89.21	4.45	6.02	9.26	6.85
0.1	55	187.2	87.73	4.14	5.75	8.84	6.38
0.15	35	178.1	83.50	4.48	8.15	12.53	6.89
0.15	45	174.3	81.72	4.23	8.01	12.32	6.51
0.15	55	169.2	79.32	4.24	8.29	12.75	6.52

Table 3.10: 3-Point Bending Stress Strain Graph



The 3-point bend test was conducted with varying combinations of layer height and print speed, and the corresponding flexure strength values were recorded. The table displays the results, indicating that a trend of decreasing flexure strength with increasing layer height can be observed within each print speed category. For instance, at a layer height of 0.06mm, the flexure strength decreased from 96.32 MPa to 95.54 MPa as the print speed increased from 35mm/s to 55mm/s. Similarly, at a layer height of 0.1mm, the flexure strength dropped from 91.02 MPa to 87.73 MPa with the same increase in print speed. This trend continues with a layer height of 0.15mm, resulting in flexure strength values decreasing from 83.5 MPa to 79.32 MPa. These findings suggest that, generally, lower layer heights result in improved flexure strength. Additionally, within each layer height, a minor fluctuation in flexure strength can be observed with varying print speeds, indicating a relatively smaller influence of print speed on mechanical performance compared to the impact of layer height.

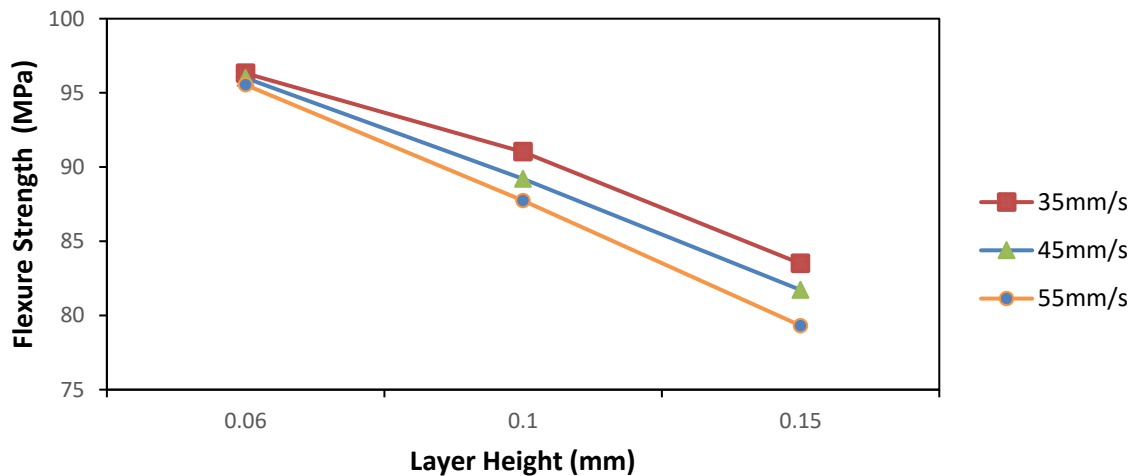


Figure 3.17: 3-Point Bending Flexure Strength Graph

When examining strain elongation percentages, it is evident that a trend of decreasing strain with an increase in print speed is notable within each layer height category. For instance, at a layer height of 0.06mm, the strain decreased from 10.19% to 8.65% as the print speed increased from 35mm/s to 55mm/s. Similarly, at a layer height of 0.1mm, the strain decreased from 9.602% to 8.84% with the same print speed increment. The strain values at 0.15mm layer height show a different behavior with varying print speeds. At this layer height, the strain percentages exhibit a slight increase as print speed rises. Specifically, the strain elongation percentages rise from 12.53% to 12.75% as the print speed escalates from 35mm/s to 55mm/s. The increased strain elongation at

higher layer heights and print speeds could be a result of the combination of layer bonding and print speed-induced cooling effects. This relationship underscores the influence of print speed on the mechanical behavior of the printed specimens during the 3-point bend test, with lower print speeds generally corresponding to higher strain elongation percentages.

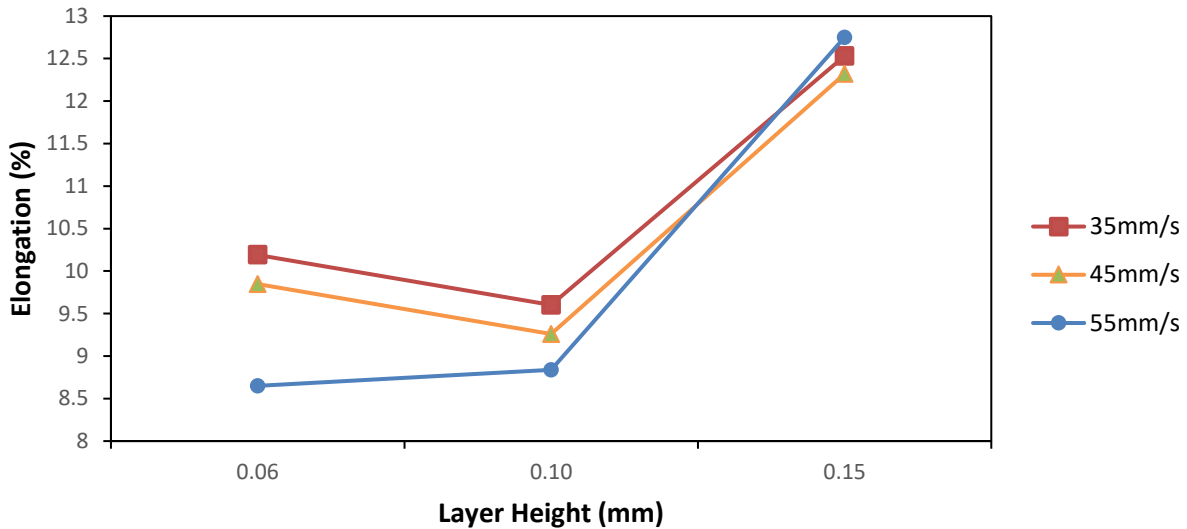


Figure 3.18: 3-Point Bending Elongation (%) Graph

3.5 Surface Roughness

3.5.1 Tensile Testing Specimen

The surface roughness of the 3D printed parts was evaluated through Tensile and 3-point bending tests, utilizing the MarSurf M 310. The device used in the study had the capability to measure a broad range of surface roughness parameters, including Ra (arithmetic average roughness), Rz (sum of maximum peak and maximum valley of a profile), and several others. Among these parameters, the arithmetic average roughness Ra was chosen as the primary roughness parameter for comparison, as it is the most commonly used and widely accepted in mechanical engineering. The examination focused on the surface roughness of both the top surface layer and the side surface, as well as the hatch distance between the top and side surface layers. The Table 3.11 illustrates the measured surface roughness values (Ra) for different specimens, and one specimen with acetone vapor exposure.

Table 3.11: Tensile Testing Specimen Surface Roughness & Hatch Distance

Layer Height (mm)	Print Speed (mm/s)	Surface Roughness (Ra)		Hatch Distances	
		Top (µm)	Side (µm)	Top (µm)	Side (µm)
0.06	35	4.03	5.42	335.616	61.169
0.06	45	6.79	4.62	351.147	64.662
0.06	55	2.50	4.24	363.383	66.408
0.1	35	3.84	6.15	345.901	106.694
0.1	45	6.04	6.69	362.107	108.439
0.1	55	1.81	6.50	375.351	108.327
0.15	35	3.15	8.22	359.894	155.726
0.15	45	3.47	7.25	375.026	157.238
0.15	55	1.59	7.78	389.075	160.772
0.15	45 (1.05T)	0.65	0.77	371.944	153.744

In the analysis of tensile testing, the print speed versus layer heights graph indicated that increasing the print speed led to slightly decrease in the Ra surface roughness for the top surface layer. At 35mm/s, the Ra values ranged from 3.15µm to 4.03µm. For 45mm/s, the Ra values were highest, ranging from 3.47µm to 6.79µm, and at 55mm/s, the Ra values were observed, ranging from 1.59µm to 2.50µm.

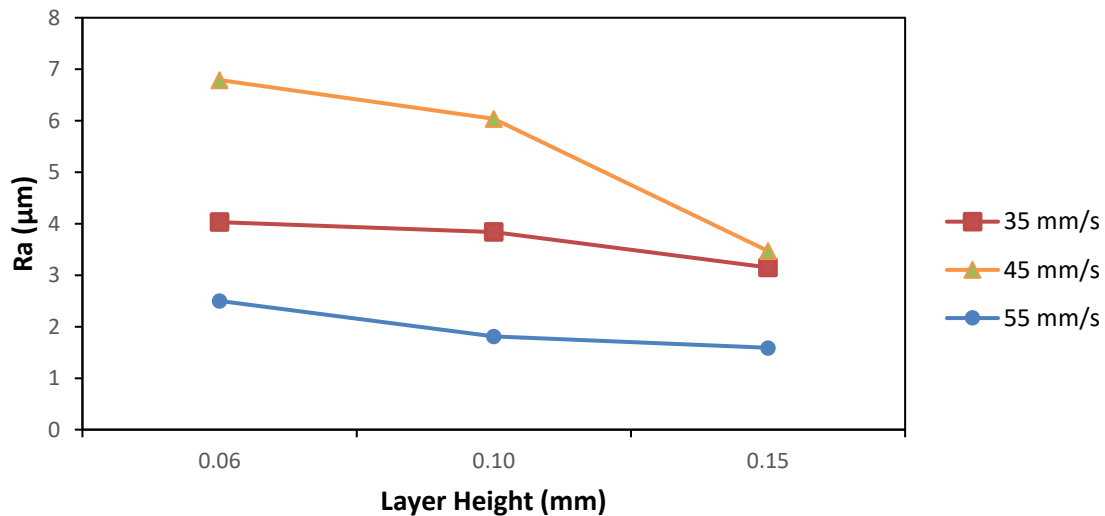


Figure 3.19: Tensile Testing Specimen Top Surface Roughness

For the side/vertical surface, both layer height and print speed showed an increase in the Ra surface roughness, with the effect of layer height being more pronounced. The lowest Sa value was observed for a layer height of 0.06 mm, while 0.1 mm had a greater value, and 0.15 mm had the highest Ra value. In essence, an increase in layer height resulted in an increase in surface roughness for the side/vertical surface.

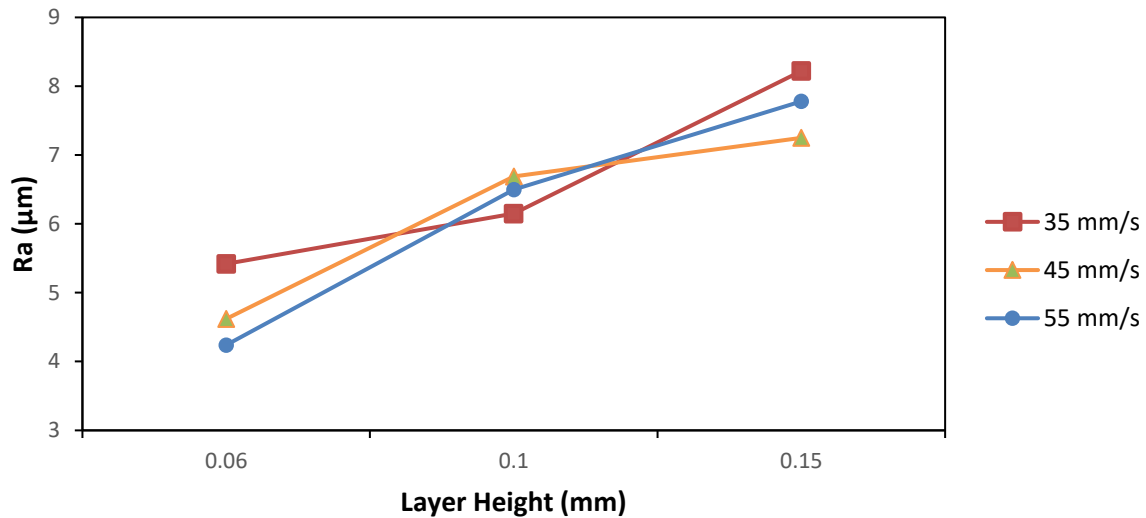


Figure 3.20: Tensile Testing Specimen Side Surface Roughness

Notably, one intriguing finding emerged when a sample test was subjected to post-processing with acetone, utilizing a layer height of 0.15 mm and a print speed of 45 mm/s. The process involves exposing the FDM parts to a solvent vapor, such as acetone, which creates a chemical reaction on the outer surface of the parts. This reaction melts and fuses the outer layers, resulting in a smoother and more uniform surface finish. The main goal is to reduce visible layer lines and improve the overall surface finish. To evaluate its effectiveness, surface roughness measurements are performed to identify the best combination of layer height and print speed for achieving smooth surfaces. This particular treatment resulted in the lowest surface roughness values observed, with Ra surface roughness measuring 0.65µm and 0.77µm for the top and side surfaces, respectively. The research findings demonstrate that acetone vapor treatment significantly improves the surface finish of FDM parts, reducing visible layer lines and smoothing surface imperfections.

The microstructural analysis revealed that the top surface hatch distance, representing the distance between adjacent layer printed paths, increased with increased print speed while

remaining slightly increases with varying layer heights. At 35 mm/s, a hatch distance equivalent to a range of 335.616 μm to 359.894 μm was observed, while 45 mm/s showed 351.147 μm to 375.026 μm , and 55 mm/s had a range value of 363.383 μm to 389.075 μm .

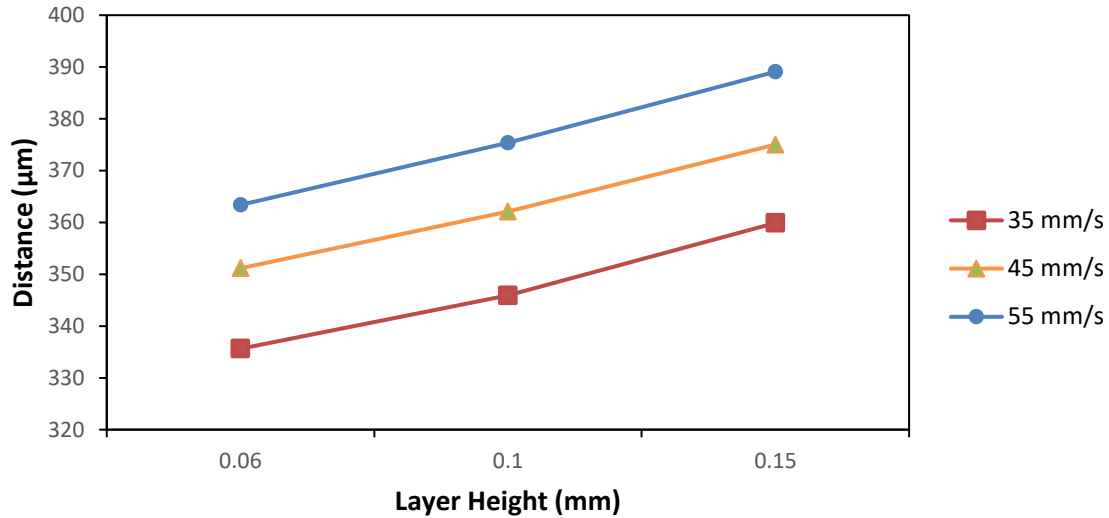


Figure 3.21: Tensile Testing Specimen Top Surface Hatch Distances

In the analysis of side/vertical hatch distance, it was observed that the hatch distance increased proportionally with the layer height, regardless of the print speed. The hatch distances were reported in micrometers and were nearly equivalent to the layer height values of 0.06 mm, 0.1 mm, and 0.15 mm.

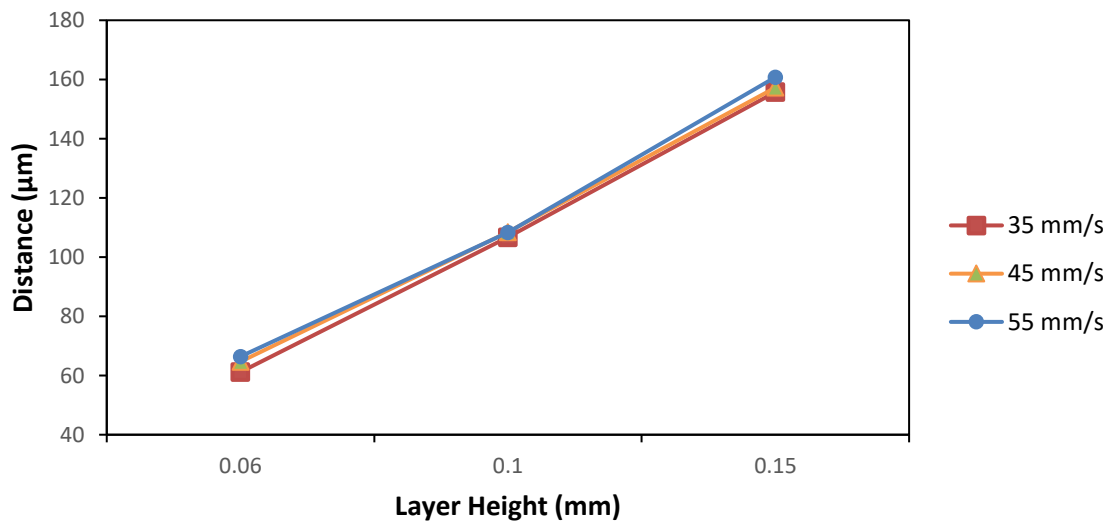


Figure 3.22: Tensile Testing Specimen Side Surface Hatch Distances

The results suggested that the hatch distance played a significant role in the surface roughness and overall quality of the 3D-printed parts. Notably, the hatch distances in both horizontal and vertical directions exhibited consistency with the 0.15 mm layer height and 45 mm/s print speed, indicating that the post-processing treatment did not significantly impact the hatch distance in this particular case. The Table 3.12 & 3.13 shows the Digital microscope images showing the hatch distance at top and side surface of the tensile test specimen.

Table 3.12: Tensile Testing Specimen Top Surface Hatch Distances

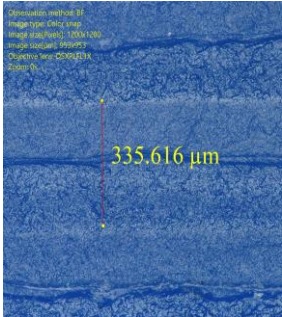
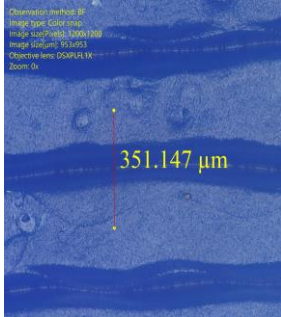
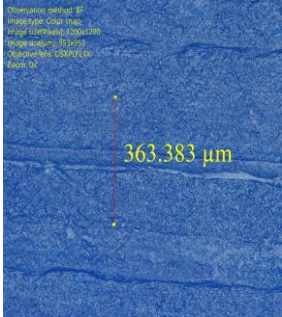
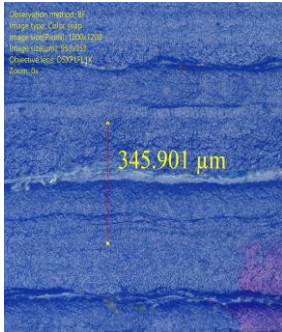
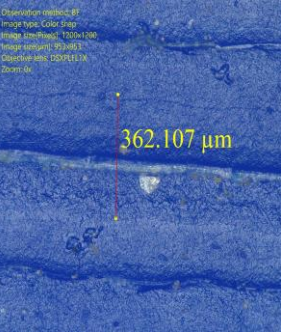
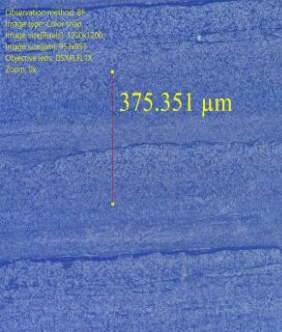
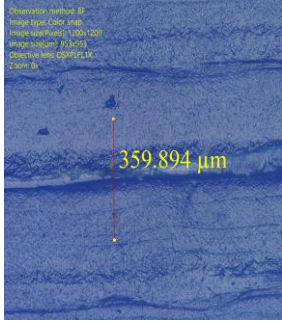
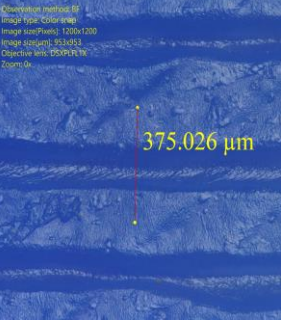
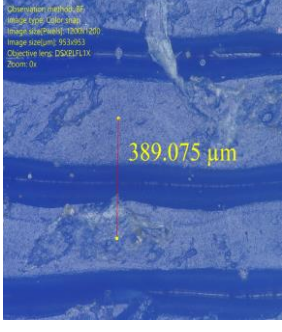
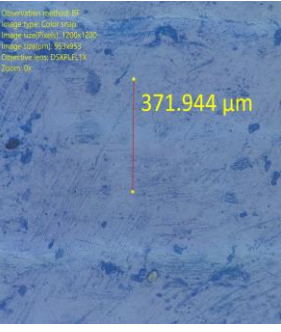
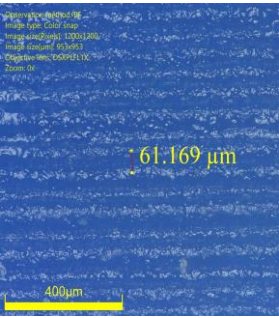
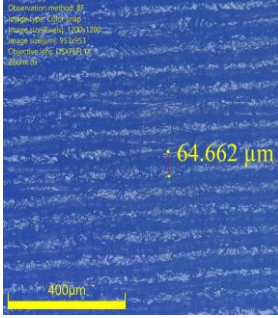
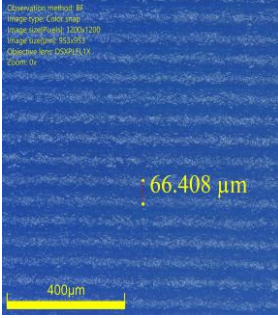
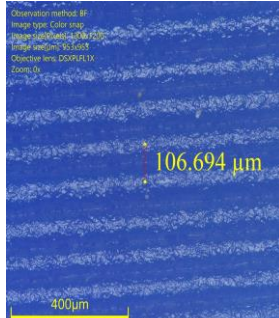
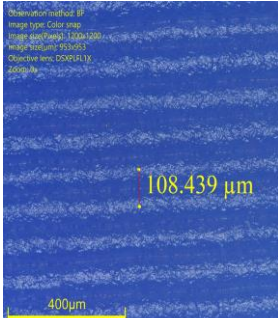
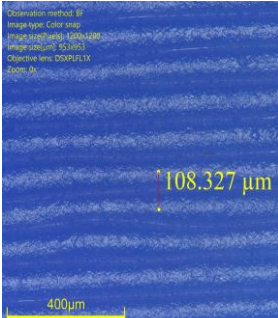
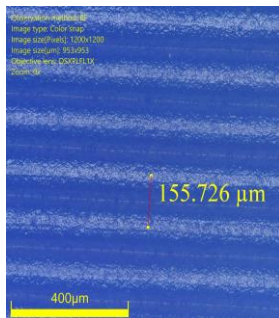
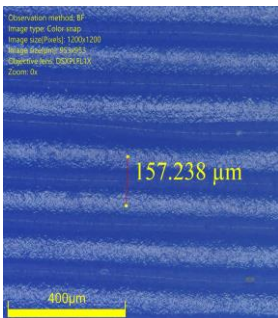
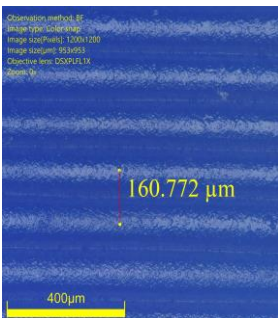
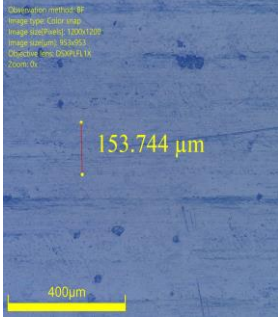
Layer Height (mm)	Print Speed (mm/s)		
	35	45	55
0.06	 <p>335.616 μm</p>	 <p>351.147 μm</p>	 <p>363.383 μm</p>
0.10	 <p>345.901 μm</p>	 <p>362.107 μm</p>	 <p>375.351 μm</p>
0.15	 <p>359.894 μm</p>	 <p>375.026 μm</p>	 <p>389.075 μm</p>
0.15 (1.05 T)		 <p>371.944 μm</p>	

Table 3.13: Tensile Testing Specimen Side Surface Hatch Distances

Layer Height (mm)	Print Speed (mm/s)		
	35	45	55
0.06	 <p>61.169 μm</p>	 <p>64.662 μm</p>	 <p>66.408 μm</p>
0.10	 <p>106.694 μm</p>	 <p>108.439 μm</p>	 <p>108.327 μm</p>
0.15	 <p>155.726 μm</p>	 <p>157.238 μm</p>	 <p>160.772 μm</p>
0.15 (1.05 T)		 <p>153.744 μm</p>	

3.5.2 3-Point Bending Specimen

The surface roughness trend in 3-point bending revealed that the combination of a 0.06mm layer height and 35mm/s print speed yielded the highest surface roughness 17.81 μ m Ra value compared to other settings. Conversely, the 0.15mm layer height and 55mm/s print speed resulted in the lowest roughness. This pattern was consistent for both top and side surfaces, as shown in Table 3.14 and Figures 3.23 to 3.26.

Table 3.14: 3-Point Bending Specimen Surface Roughness & Hatch Distance

Layer Height (mm)	Print Speed (mm/s)	Surface Roughness (Ra)		Hatch Distances	
		Top (μ m)	Side (μ m)	Top (μ m)	Side (μ m)
0.06	35	17.81	4.69	331.957	59.432
0.06	45	9.96	5.36	346.06	66.477
0.06	55	8.99	5.30	361.73	64.662
0.10	35	5.91	4.87	345.774	106.694
0.10	45	3.07	5.73	361.641	104.95
0.10	55	1.90	5.99	372.616	106.627
0.15	35	2.96	8.19	360.881	153.774
0.15	45	2.10	7.10	374.759	157.383
0.15	55	1.91	8.81	388.238	157.238

The surface roughness of the top of the 3-point bending specimen demonstrates that the print speed has a greater impact on Ra surface roughness compared to the layer height, aligning with similar outcomes seen in the surface roughness of the top of the tensile test specimen.

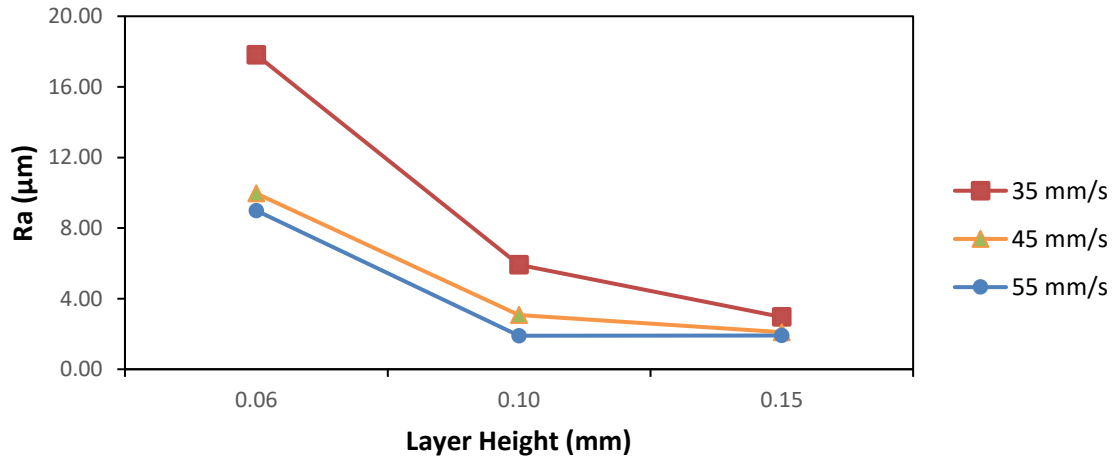


Figure 3.23: 3-Point Bending Specimen Top Surface Roughness

The side surface roughness of the 3-point bending specimen follows comparable patterns to the results from the tensile testing specimen. In terms of determining Ra surface roughness, the layer height has a more noticeable influence compared to the print speed, as shown in Figure 3.24.

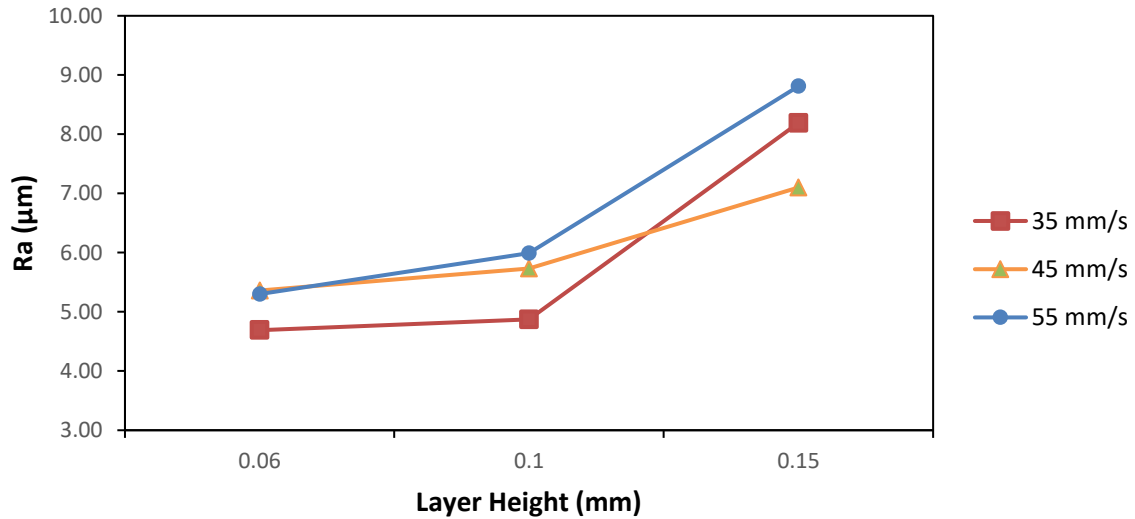


Figure 3.24: 3-Point Bending Specimen Side Surface Roughness

In the 3-point bending test, the hatch distances for both the top and side surfaces display similar outcomes to the results of the tensile testing. The trend of hatch distances is consistent, and the values are comparable to those observed in the tensile test for both top and side surfaces, as illustrated in Table 3.15 and 3.16, as well as Figures 3.25 and 3.26.

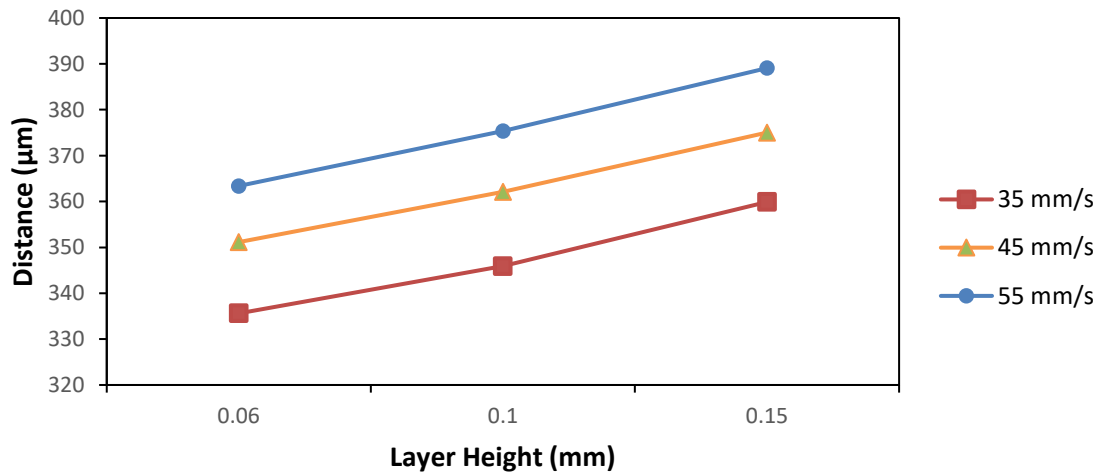


Figure 3.25: 3-Point Bending Specimen Top Surface Hatch Distances

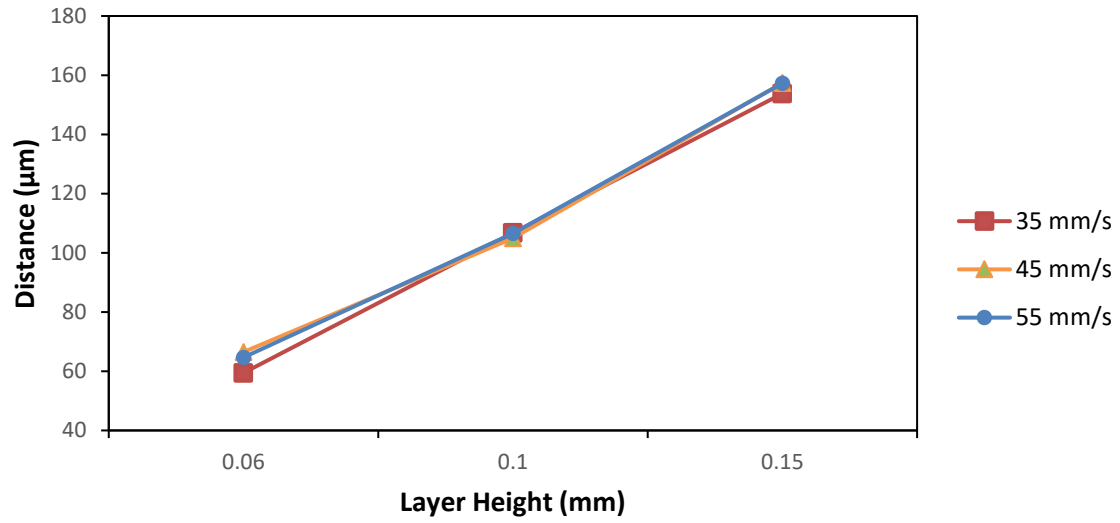


Figure 3.26: 3-Point Bending Specimen Side Surface Hatch Distances

Table 3.15: 3-Point Bending Specimen Top Surface Hatch Distances

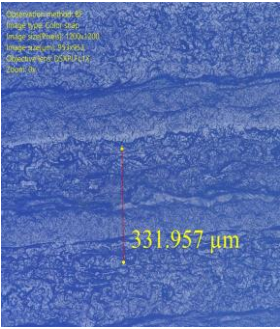
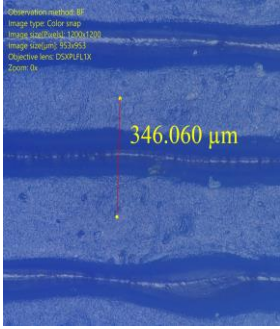
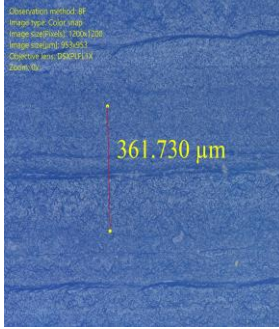
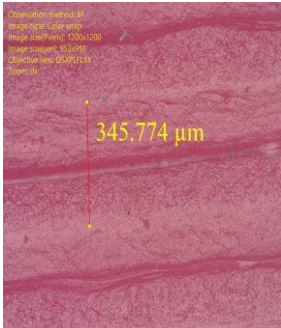
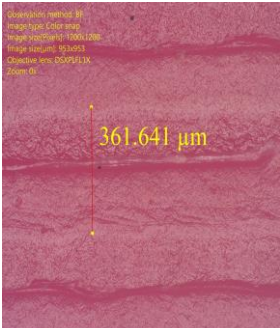
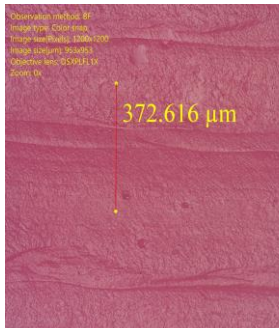
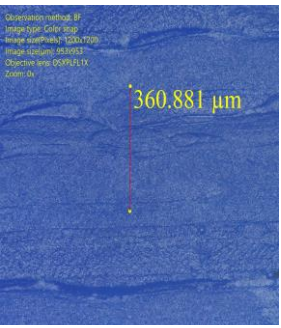
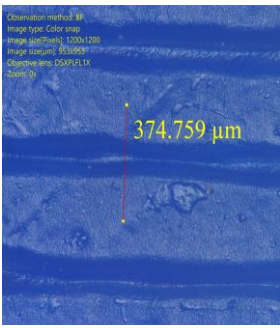
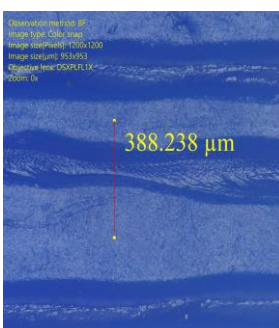
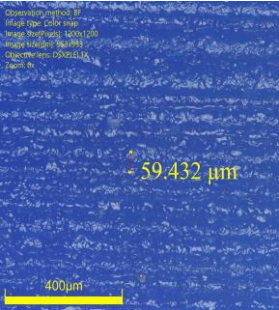
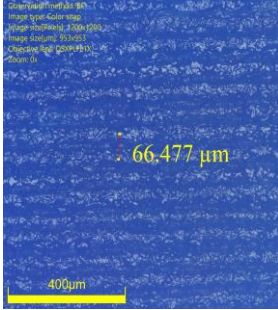
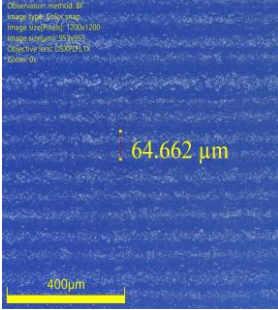
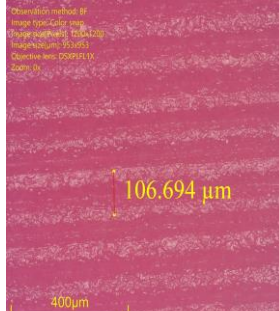
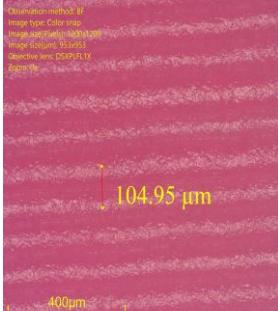
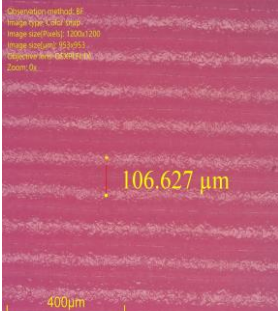
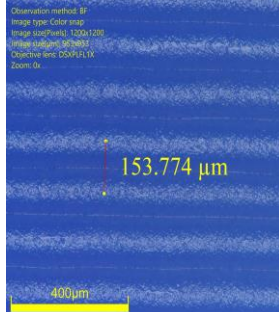
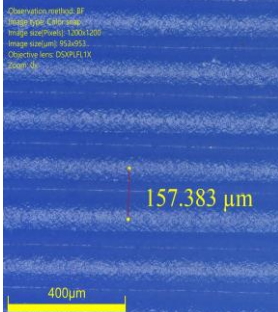
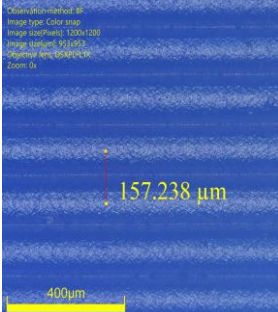
3-Point Bending Specimen Top Surface Hatch Distances			
Layer Height (mm)	Print Speed (mm/s)		
	35	45	55
0.06	 <p>331.957 μm</p>	 <p>346.060 μm</p>	 <p>361.730 μm</p>
0.10	 <p>345.774 μm</p>	 <p>361.641 μm</p>	 <p>372.616 μm</p>
0.15	 <p>360.881 μm</p>	 <p>374.759 μm</p>	 <p>388.238 μm</p>

Table 3.16: 3-Point Bending Specimen Side Surface Hatch Distances

Layer Height (mm)	Print Speed (mm/s)		
	35	45	55
0.06			
0.10			
0.15			

CHAPTER 4: CONCLUSION

From the research conducted, several significant insights were drawn regarding 3D printing parameters and their impact on part quality. The key parameters of layer height and print speed were identified as pivotal factors influencing the final outcomes. Regarding dimensional accuracy, it was found that employing an extra fine layer height in combination with the lowest print speed led to exceptional precision, achieving an impressive 79.32% accuracy within the defined tolerance range. Notably, when considering different print speeds, a speed of 35mm/s exhibited the highest tolerance percentage. However, as layer height and print speed were increased, there was a subsequent decrease in dimensional accuracy. In terms of fine feature size, the research revealed that while 0.5mm features were printable with a certain degree of higher print error, 0.25mm features were not feasible across all parameter variations. Strength analysis showed that the maximum tensile and flexure strength were attained using an extra fine layer height (0.06mm) and the slowest print speed (35mm/s). On the other hand, strength diminished as layer height and print speed increased. Surface roughness was influenced by these parameters as well; the top surface roughness (Ra) decreased with increase in layer height and print speed, while side surface roughness increased with these factors. Acetone vapor treatment effectively reduced roughness, transforming the initial Ra value of 1.59 μ m to 0.65 μ m. Interestingly, this treatment exhibited negligible impact on mechanical strength but resulted in observable changes in elongation percentage. Hatch distance alterations yielded insights into top and side surface textures. For the top surface, hatch distance slightly increased within the micro level range (330 μ m to 390 μ m) due to higher layer height and print speed. Conversely, side surface hatch distance correlated with layer height, regardless of print speed. Furthermore, it was apparent that layer thickness held greater effect over mechanical properties and printing time when compared to print speed.

REFERENCES

- [1] Rouf, S., Malik, A., Singh, N., Raina, A., Naveed, N., Siddiqui, M. I. H., and Haq, M. I. U., 2022, “Additive Manufacturing Technologies: Industrial and Medical Applications,” *Sustainable Operations and Computers*, **3**, pp. 258–274.
- [2] Song, X. T., Kuo, J.-Y., and Chen, C.-H., 2022, “Chapter 3 - Design Methodologies for Conventional and Additive Manufacturing,” ScienceDirect, pp. 97–143 [Online]. Available:
<https://www.sciencedirect.com/science/article/abs/pii/B9780323950626000073>.
[Accessed: 09-Jun-2023].
- [3] Stentoft, J., Philipsen, K., Haug, A., and Wickstrøm, K. A., 2020, “Motivations and Challenges with the Diffusion of Additive Manufacturing through a Non-Profit Association,” *Journal of Manufacturing Technology Management*.
- [4] Dey, A., and Yodo, N., 2019, “A Systematic Survey of FDM Process Parameter Optimization and Their Influence on Part Characteristics,” *Journal of Manufacturing and Materials Processing*, **3**(3), p. 64.
- [5] Ngo, T. D., Kashani, A., Imbalzano, G., Nguyen, K. T. Q., and Hui, D., 2018, “Additive Manufacturing (3D Printing): A Review of Materials, Methods, Applications and Challenges,” *Composites Part B: Engineering*, **143**, pp. 172–196.
- [6] Tofail, S. A. M., Koumoulos, E. P., Bandyopadhyay, A., Bose, S., O’Donoghue, L., and Charitidis, C., 2018, “Additive Manufacturing: Scientific and Technological Challenges, Market Uptake and Opportunities,” *Materials Today*, **21**(1), pp. 22–37.
- [7] Iftekar, S. F., Aabid, A., Amir, A., and Baig, M., 2023, “Advancements and Limitations in 3D Printing Materials and Technologies: A Critical Review,” *Polymers*, **15**(11), p. 2519.
- [8] Fayazfar, H., Salarian, M., Rogalsky, A., Sarker, D., Russo, P., Paserin, V., and Toyserkani, E., 2018, “A Critical Review of Powder-Based Additive Manufacturing of Ferrous Alloys: Process Parameters, Microstructure and Mechanical Properties,” *Materials & Design*, **144**, pp. 98–128.
- [9] Vahid Monfared, Ramakrishna, S., Navid Nasajpour-Esfahani, Davood Toghraie, Maboud Hekmatifar, and Rahmati, S., 2023, “Science and Technology of Additive Manufacturing Progress: Processes, Materials, and Applications.”

- [10] Javaid, M., Haleem, A., Singh, R. P., Suman, R., and Rab, S., 2021, "Role of Additive Manufacturing Applications towards Environmental Sustainability," *Advanced Industrial and Engineering Polymer Research*, **4**(4).
- [11] Shim, D., 2021, "Effects of Process Parameters on Additive Manufacturing of Aluminum Porous Materials and Their Optimization Using Response Surface Method," *Journal of Materials Research and Technology*, **15**, pp. 119–134.
- [12] Moradi, M., Meiabadi, S., and Kaplan, A., 2019, "3D Printed Parts with Honeycomb Internal Pattern by Fused Deposition Modelling; Experimental Characterization and Production Optimization," *Metals and Materials International*, **25**(5), pp. 1312–1325.
- [13] Dey, A., Roan Eagle, I. N., and Yodo, N., 2021, "A Review on Filament Materials for Fused Filament Fabrication," *Journal of Manufacturing and Materials Processing*, **5**(3), p. 69.
- [14] Masood, S. H., 2014, "10.04 - Advances in Fused Deposition Modeling," *ScienceDirect*, pp. 69–91 [Online]. Available: <https://www.sciencedirect.com/science/article/abs/pii/B9780080965321010025>. [Accessed: 09-Jun-2023].
- [15] Garzon-Hernandez, S., Garcia-Gonzalez, D., Jérusalem, A., and Arias, A., 2020, "Design of FDM 3D Printed Polymers: An Experimental-Modelling Methodology for the Prediction of Mechanical Properties," *Materials & Design*, **188**, p. 108414.
- [16] Penumakala, P. K., Santo, J., and Thomas, A., 2020, "A Critical Review on the Fused Deposition Modeling of Thermoplastic Polymer Composites," *Composites Part B: Engineering*, **201**, p. 108336.
- [17] Velu, R., Jayashankar, D. K., and Subburaj, K., 2021, "Chapter 20 - Additive Processing of Biopolymers for Medical Applications," *ScienceDirect*, pp. 635–659 [Online]. Available: <https://www.sciencedirect.com/science/article/abs/pii/B9780128184110000197>. [Accessed: 09-Jun-2023].
- [18] Mohammed, A. A., Algahtani, M. S., Ahmad, M. Z., Ahmad, J., and Kotta, S., 2021, "3D Printing in Medicine: Technology Overview and Drug Delivery Applications," *Annals of 3D Printed Medicine*, **4**, p. 100037.

- [19] Kim, S., Seong, H., Her, Y., and Chun, J., 2019, “A Study of the Development and Improvement of Fashion Products Using a FDM Type 3D Printer,” *Fashion and Textiles*, **6**(1).
- [20] Ali, Md. H., Kurokawa, S., Shehab, E., and Mukhtarkhanov, M., 2023, “Development of a Large-Scale Multi-Extrusion FDM Printer, and Its Challenges,” *International Journal of Lightweight Materials and Manufacture*, **6**(2), pp. 198–213.
- [21] Mathew, A., Kishore, S. R., Tomy, A. T., Sugavaneswaran, M., Scholz, S. G., Elkaseer, A., Wilson, V. H., and John Rajan, A., 2023, “Vapour Polishing of Fused Deposition Modelling (FDM) Parts: A Critical Review of Different Techniques, and Subsequent Surface Finish and Mechanical Properties of the Post-Processed 3D-Printed Parts,” *Progress in Additive Manufacturing*.
- [22] Montez, M., Willis, K., Rendler, H., Marshall, C., Rubio, E., Rajak, D. K., Rahman, M. H., and Menezes, P. L., 2022, “5 - Fused Deposition Modeling (FDM): Processes, Material Properties, and Applications,” *ScienceDirect*, pp. 137–163 [Online]. Available: <https://www.sciencedirect.com/science/article/abs/pii/B9780128213285000056>. [Accessed: 09-Jun-2023].
- [23] Dizon, J. R. C., Gache, C. C. L., Cascolan, H. M. S., Cancino, L. T., and Advincula, R. C., 2021, “Post-Processing of 3D-Printed Polymers,” *Technologies*, **9**(3), p. 61.
- [24] Syrlybayev, D., Zharylkassyn, B., Seisekulova, A., Perveen, A., and Talamona, D., 2021, “Optimization of the Warp of Fused Deposition Modeling Parts Using Finite Element Method,” *Polymers*, **13**(21), p. 3849.
- [25] Mazzanti, V., Malagutti, L., and Mollica, F., 2019, “FDM 3D Printing of Polymers Containing Natural Fillers: A Review of Their Mechanical Properties,” *Polymers*, **11**(7), p. 1094.
- [26] Podsiadły, B., Skalski, A., Rozpiórski, W., and Słoma, M., 2021, “Are We Able to Print Components as Strong as Injection Molded?—Comparing the Properties of 3D Printed and Injection Molded Components Made from ABS Thermoplastic,” *Applied Sciences*, **11**(15), p. 6946.
- [27] Song, R., Telenko, C., and Woodruff, G., 2016, *MATERIAL WASTE of COMMERCIAL FDM PRINTERS under REALSTIC CONDITIONS*.

- [28] Jain, R., Shivansh Nauriyal, Gupta, V., and Khas, K. S., 2021, “Effects of Process Parameters on Surface Roughness, Dimensional Accuracy and Printing Time in 3D Printing,” pp. 187–197.
- [29] Wang, P., Zou, B., Ding, S., Li, L., and Huang, C., 2020, “Effects of FDM-3D Printing Parameters on Mechanical Properties and Microstructure of CF/PEEK and GF/PEEK,” *Chinese Journal of Aeronautics*.
- [30] Abeykoon, C., Sri-Amphorn, P., and Fernando, A., 2020, “Optimization of Fused Deposition Modeling Parameters for Improved PLA and ABS 3D Printed Structures,” *International Journal of Lightweight Materials and Manufacture*, **3**(3), pp. 284–297.
- [31] Frunzaverde, D., Cojocar, V., Ciubotariu, C.-R., Miclosina, C.-O., Ardeljan, D. D., Ignat, E. F., and Marginean, G., 2022, “The Influence of the Printing Temperature and the Filament Color on the Dimensional Accuracy, Tensile Strength, and Friction Performance of FFF-Printed PLA Specimens,” *Polymers*, **14**(10), p. 1978.
- [32] Mwema, F. M., and Akinlabi, E. T., 2020, “Basics of Fused Deposition Modelling (FDM),” *Fused Deposition Modeling*, pp. 1–15.
- [33] Liu, C.-H., and Hung, P.-T., 2022, “Effect of the Infill Density on the Performance of a 3D-Printed Compliant Finger,” *Materials & Design*, **223**, p. 111203.
- [34] Jiang, J., Xu, X., and Stringer, J., 2018, “Support Structures for Additive Manufacturing: A Review,” *Journal of Manufacturing and Materials Processing*, **2**(4), p. 64.
- [35] Sagias, V D, K I Giannakopoulos, and C Stergiou. 2018. “Mechanical Properties of 3D Printed Polymer Specimens.” *Procedia Structural Integrity* 10: 85–90. <https://www.sciencedirect.com/science/article/pii/S2452321618300611>.
- [36] Ultimaker. 2018. “Mechanical Properties Injection Molding 3D Printing Technical Data Sheet ABS.” : 1–3. https://support.ultimaker.com/hc/en-us/article_attachments/360010199279/TDS_ABS_v3.011_-en.pdf.
- [37] ASTM-D882-12. 2014. “Standard Test Method for Tensile Properties of Plastics.” *ASTM Standards* 08.
- [38] ASTM INTERNATIONAL. 2002. “Standard Test Methods for Flexural Properties of Unreinforced and Reinforced Plastics and Electrical Insulating Materials. D790.” *Annual Book of ASTM Standards*: 1–12.

- [39] Chacón, J. M., M. A. Caminero, E. García-Plaza, and P. J. Núñez. 2017. “Additive Manufacturing of PLA Structures Using Fused Deposition Modelling: Effect of Process Parameters on Mechanical Properties and Their Optimal Selection.” *Materials and Design* 124: 143–57. <http://dx.doi.org/10.1016/j.matdes.2017.03.065>.
- [40] Mac, Gary, Hammond Pearce, Ramesh Karri, and Nikhil Gupta. 2021. “Uncertainty Quantification in Dimensions Dataset of Additive Manufactured NIST Standard Test Artifact.” *Data in Brief* 38: 107286. <https://doi.org/10.1016/j.dib.2021.107286>.
- [41] Kubatova, Dana, and Aneta Kaufnerova. 2021. “3D Scanning - Accuracy of a Volume Model Transformed From Scanned Data.” *Annals of DAAAM and Proceedings of the International DAAAM Symposium* 32(1): 140–44.